Title
STUDIES OF FISSION IN HEAVY ELEMENTS UNDER HIGH-ENERGY BOMBARDMENTS

Author
Steiner, Herbert M.

Publication Date
1956-01-12

UCRL 3258

UNIVERSITY OF CALIFORNIA

Radiation Laboratory

BERKELEY, CALIFORNIA

DISCLAIMER

UCRL-3258

UNIVERSITY OF CALIFORNIA
Radiation Laboratory
Berkeley, California

Contract No. W-7405-eng-48

STUDIES OF FISSION IN HEAVY ELEMENTS UNDER HIGH-ENERGY BOMBARDMENTS

Herbert M. Steiner

(Thesis)

January 12, 1956

Printed for the U.S. Atomic Energy Commission

STUDIES OF FISSION IN HEAVY ELEMENTS UNDER HIGH-ENERGY BOMBARDMENTS

Contents

Abstract 4

Introduction 5

Charged-Particle Experiments on Uranium-238, Uranium-235, Thorium-232, Bismuth-209, and Gold-197

I. Introduction 7

II. Apparatus

A. Fission Detector 8

B. Samples 12

C. Beam Monitor 14

III. Experimental Method

A. Arrangement 14

B. Procedure

1. Alignment 17

2. Variation of High Voltage on Electrodes B and C 17

3. Background and Cancellation 18

4. Pile-Up of Fission Pulses 18

5. Gating of Scalers 20

6. Geometry of Fission Chamber . . . 20

7. Neutrons 21

8. Momentum Transfer to Struck Nucleus 21

IV. Results 27

V. Discussion

A. Energy Dependence of Fission Cross Section . 46

B. Comparison to Total Inelastic Cross Section . 46

C. Dependence of the Fission Cross Section on the Atomic Number of the Target Nucleus . 50

D. Excitation Energy of the Struck Nucleus . . . 50

E. Comparison to Other Experiments 51

F. Applications 51

Contents (continued)

Charged-Particle Experiments on Uranium-233, Uranium-234, Uranium-236, and Neptunium-237

I. Introduction 50

II. Apparatus

A. Samples 50

III. Procedure 54

IV. Results 55

V. Discussion 55

Photofission Experiments

I. Introduction 57

II. Apparatus and Method

A. Fission Chamber 57

B. Samples 58

C. Method 58

III. Procedure

A. Slow Neutrons 61

B. Alignment 61

C. Cancellation 61

D. Pile-Up of Fission Pulses 62

E. Variation of High Voltage on Electrodes B and C 62

F. Integral Bias Curve 62

G. Gating of Scalers 62

H. Neutrons 63

I. Electron Contamination 63

IV. Experimental Results 65

V. Discussion

A. Bismuth and Gold 71

B. Uranium-238, Uranium-235, and Thorium-232 . 73

Acknowledgments 75

Appendix I 76

Appendix II 77

Bibliography 79

STUDIES OF FISSION IN HEAVY ELEMENTS UNDER HIGH-ENERGY BOMBARDMENTS

Herbert M. Steiner

Radiation Laboratory
University of California
Berkeley, California

January 12, 1956

ABSTRACT

We have measured the total fission cross sections of several heavy elements for high-energy protons, deuterons, alpha particles, and photons. The energies of the bombarding particles ranged from 100 to 500 Mev. A cancellation-type ionization chamber was used to detect the fission fragments. In the charged-particle-induced fission experiments, the measured fission cross sections were compared to the total inelastic cross sections in order to determine the fission probability as a function of the energy and of the type of incident particle. The photofission results indicate that a possible mechanism for the production of fission by high-energy photons is through the production and subsequent reabsorbtion of photomesons.

STUDIES OF FISSION IN HEAVY ELEMENTS UNDER HIGH-ENERGY BOMBARDMENTS

Herbert M. Steiner

Radiation Laboratory
University of California
Berkeley, California

January 12, 1956

INTRODUCTION

With the advent of high-energy accelerators it became possible to study the fission of heavy elements by high-energy (greater than a few Mev) particles and photons. These experiments may be divided into two general classes: (1) chemical investigations of the mass yields, which were sometimes integrated to give total cross sections, and (2) direct physical measurements of the angular distribution of the fission fragments, the distribution of the ionizing energies of the fragments, and the total fission cross sections. The experiment reported here falls into the second classification and was designed to measure the total fission cross sections of several heavy elements for high-energy charged particles and photons (100 to 500 Mev).

These cross sections are of interest for several reasons: (1) comparison of the fission cross section to the total inelastic cross section gives the relative fission probability or channel width for fission as a function of energy; (2) conversely, if the probability for fission is known, then a measure of the fission cross section will give the total cross section, which is of particular interest in photonuclear reactions; and (3) the shape of the cross-section curve as a function of energy may suggest mechanisms by which the nucleus is excited to the act of fission.

The experiment here described is subdivided into two general parts; (1) charged-particle-induced fission, and (2) photofission. The charged-particle experiments are further subdivided into (a) the measurement of the total fission cross sections of U^{238}, U^{235}, Th, Bi, and Au, and (b) the measurement of the fission cross sections of several rare isotopes such as U^{233}, U^{234}, U^{236}, and Np^{237}. This additional

subdivision was made because for the rare isotopes procedures slightly different from those used with the more common isotopes were used, both in the preparation of the samples and in the measurement of the cross sections.

CHARGED-PARTICLE EXPERIMENTS ON URANIUM-238, URANIUM-235, THORIUM-232, BISMUTH-209, AND GOLD-197

I. INTRODUCTION

In recent years several experiments have been carried out in the general field of high-energy charged-particle-induced fission in heavy elements.[1-38] Most of these experiments were designed primarily to measure the mass yield distribution of fission products as a function of the energy of the bombarding particles. In some cases the yields were integrated to give total fission cross sections; however, these were usually subject to rather large errors because of uncertainty in absolute counting of beta activities and also in beam-monitor calibration. The experiment described here was designed to measure the total fission cross sections of U^{238}, U^{235}, Th^{232}, Bi^{209}, and Au^{197} for protons, alpha particles, and deuterons by using a cancellation-type fission chamber to detect the ionization produced by the fission fragments. It was considered of interest to compare these fission cross sections with the total inelastic cross sections for the above elements in order to determine how the fission probability changed as a function of the energy and type of incident particle.

The source of charged particles used in this experiment was the 184-inch synchrocyclotron at the University of California Radiation Laboratory. The cross sections were measured in the energy region from (a) 100 to 340 Mev for protons, (b) 200 to 400 Mev for alpha particles, and (c) 70 to 190 Mev for deuterons.

II. APPARATUS

A. Fission Detector

A cancellation-type ionization chamber of 2π geometry filled with 1 atmosphere of hydrogen gas was used to detect the fission fragments. This type of fission chamber was first used by Baldwin and Klaiber,[39] and was independently suggested by Wiegand and used by Jungerman[10] for charged-particle fission studies. As shown in Fig. 1, it consisted of three electrodes, A, B, and C, arranged so as to form two adjacent parallel-plate ionization chambers of approximately equal capacitance. The spacing between the electrodes was 4.5 centimeters, and under usual operating conditions plate A was operated at zero potential, plate B at about + 1500 volts, and plate C at about + 3300 volts. Electrode B, which served as the high-voltage electrode of chamber B-C, was coupled by means of a 100-$\mu\mu$f capacitor to the grid of the first tube of a preamplifier. When equal amounts of ionization were produced simultaneously in both regions A-B and B-C, the net signal on electrode B could be made less than 1% of the ionization pulse from one region alone. A beam of charged particles passing through the fission chamber produced almost equal amounts of ionization in both these regions if care was taken to make the electrodes as thin as possible. The high-voltage electrodes were therefore made out of 140 $\mu g/cm^2$ of aluminum foil. The degree of cancellation could be adjusted by varying the high voltage on electrode C. This affected the saturation in the region B-C, so that under optimum conditions almost complete cancellation of the pulses caused by the beam ionization could be obtained. (See Figs. 2 and 3.) Upon achievement of the best possible cancellation, a sample of fissionable material was placed in the beam at electrode A. The ionization produced by a fission fragment did not cancel for two reasons: (a) the range of a fission fragment in hydrogen is about 7 to 9 cm,[40] so that most of the fragment spent all of their range in the region A-B; (b) a fission fragment ionizes most heavily at the beginning of its path, so that even if the fragment were to get into the cancellation region B-C, it would already have lost most of its energy in the region A-B. The beam usually entered the chamber in the direction C-B-A, so that most of

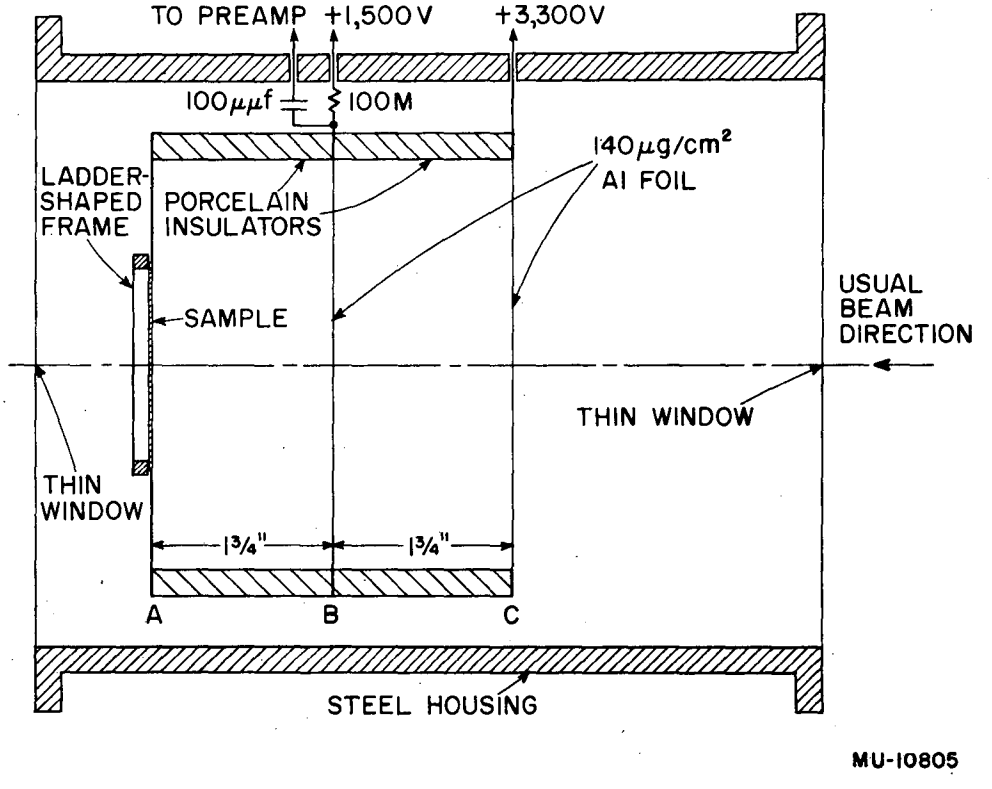

Fig. 1. Schematic drawing of the cancellation-type ionization chamber used to detect the fission fragments.

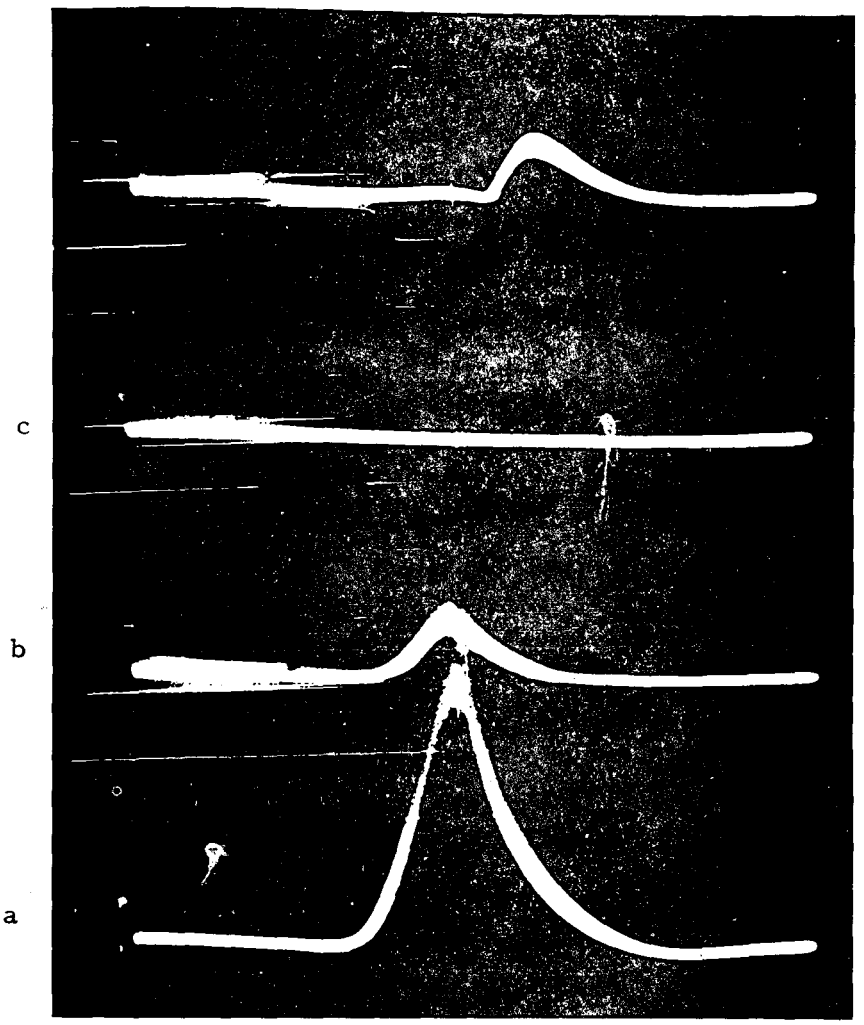

Fig. 2. Photograph showing typical pulses observed in an oscilloscope during various stages of cancellation of the pulses due to beam ionization. The cancellation of the beam pulses was adjusted by varying the voltage on electrode C with respect to electrodes A and B.

(a) A = 0 volts, B = 1500 volts, C = 1750 volts; beam pulse largely uncancelled.
(b) A = 0 volts, B = 1500 volts, C = 3000 volts; beam pulse almost cancelled.
(c) A = 0 volts, B = 1500 volts, C = 3290 volts; minimum beam signal.
(d) A = 0 volts, B = 1500 volts, C = 4500 volts; beam pulse reappears with opposite sign.

A fission pulse on same scale would be approximately 2 cm high on the oscilloscope (full scale ~4 cm).

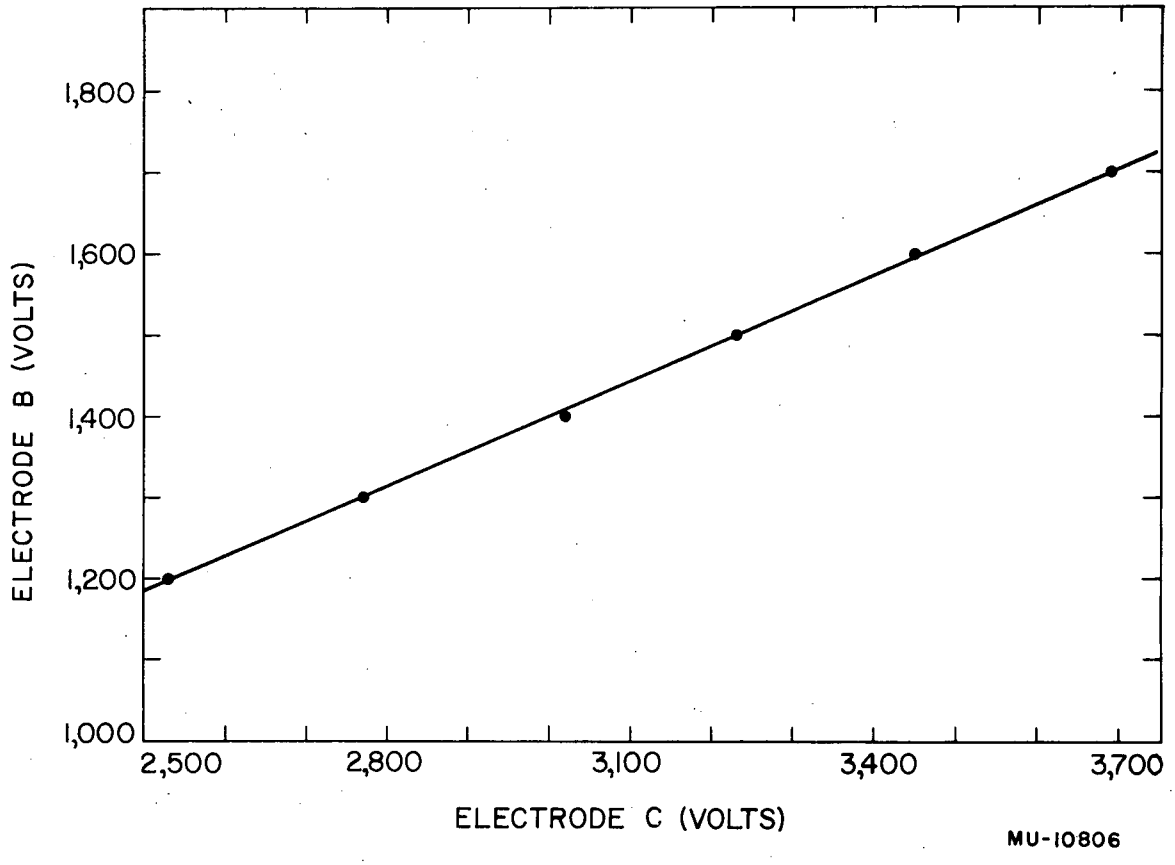

Fig. 3. Voltage on electrode B (collector) versus voltage on electrode C (cancellation) in order to achieve the best possible cancellation of pulses caused by beam ionization in the fission chamber.

the reaction products made by the beam in the 0.001-inch aluminum sample backing were knocked out of the sensitive part of the ionization chamber. Approximately four times as many background pulses were observed when the orientation of the chamber was reversed.

The signal from the preamplifier was fed into a linear pulse amplifier that had a clipping time of 5 microseconds. From there it was distributed into six scalers whose voltage discriminators were set a 5, 7.5, 10, 12.5, 15 and 20 volts respectively under usual operating conditions. In this way a counting-rate-versus-bias curve was obtained at each point. (See Fig. 4.) The true counting rate was obtained by extrapolating this curve to zero bias.

The pulses recorded as fission pulses in these experiments were observed to have the same form and magnitude as slow-neutron-induced fission pulses. Such pulses were observed with the above-described chamber when a Po-Be source encased in paraffin was placed adjacent to the fission chamber with the U^{235} sample in place.

B. Samples

The samples were prepared by either painting or evaporating the fissionable materials onto pieces of 0.001-inch aluminum foil. The areas of all samples were about 2 by 2 inches. The painting technique is described elsewhere.[41,42,43] The thickness of each sample was determined by both alpha counting and weighing whenever possible, and by weighing only for bismuth and gold. To check for uniformity in alpha-active samples all but a 0.75-cm^2 area of each sample was masked, and the exposed part of the sample was then alpha counted. The emission of alpha particles was measured with an ionization chamber from about six regions on the surface of each sample. The alpha activity in all cases was found to be uniform to within ± 3%. For U^{238} both painted and evaporated samples were prepared and used. No difference was observed between the cross sections for the painted and evaporated samples. Also, for uranium, a quantitative chemical analysis of two samples was made which showed agreement, within the experimental error of 3%, with the thicknesses as determined by alpha counting. All the targets used ranged in thickness from

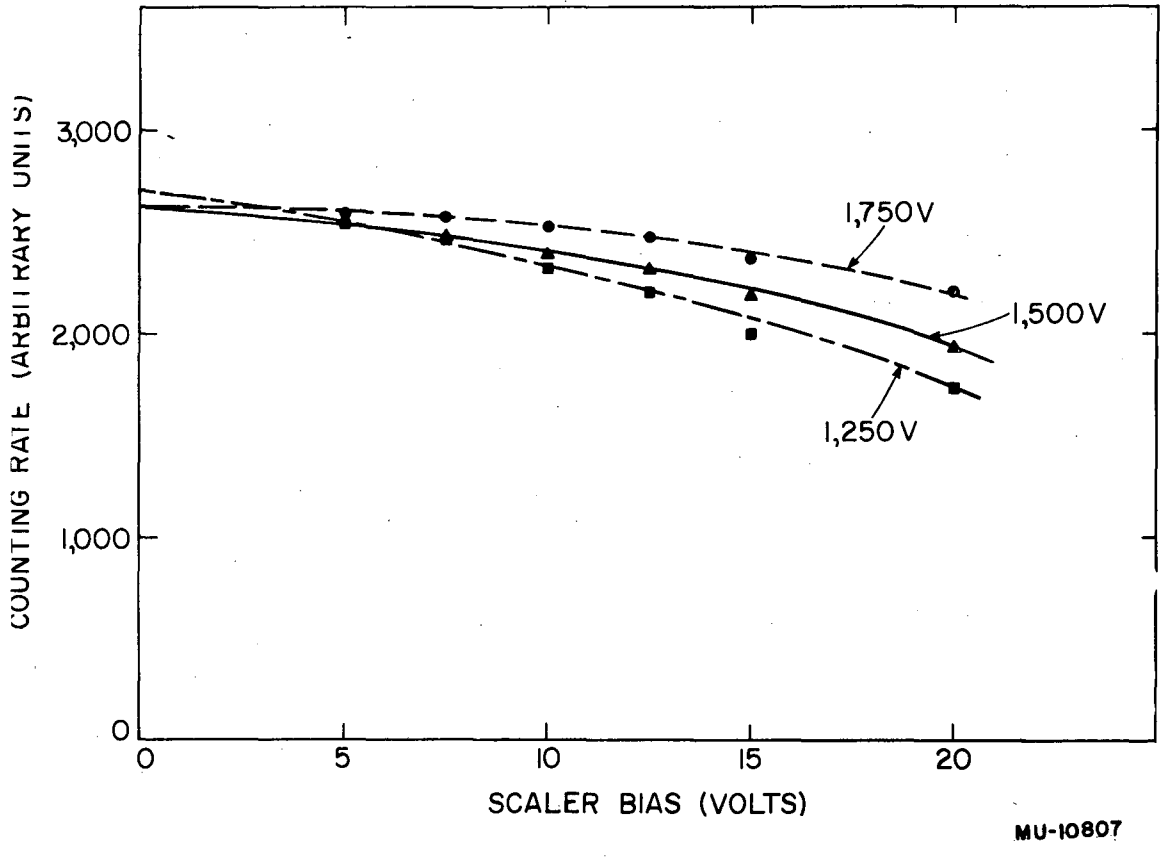

Fig. 4. Integral bias curves for various voltages on the collector electrode (electrode B). Electrode C was always adjusted to give the best possible cancellation of beam pulses. (See Fig. 3).

0.6 to 1.1 mg/cm^2 (Table I). In order to correct for sample-thickness effects, thinner samples of U^{238}, Th, Bi, and Au were also prepared. These samples ranged from 0.1 to 0.4 mg/cm^2 in thickness. Cross sections were measured by using these thin samples with protons having an energy of 336 Mev. These results were compared with the cross sections as measured with the thicker samples. In this way sample-thickness correction factors were determined for the thicker samples. It was assumed that these sample-thickness corrections were independent of the energy and of the type of beam. The sample-thickness correction factors used in these experiments ranged between 8% and 14%. (Table I).

C. Beam Monitor

The beam was monitored by a parallel-plate ionization chamber filled with one atmosphere of argon. This method of monitoring the beam is described in detail by Chamberlain, Segrè, and Wiegand.[44] The accuracy of the beam calibration using the above method is estimated to be ± 3%.

III. EXPERIMENTAL METHOD

A. Arrangement

The general experimental arrangement is shown in Fig. 5. The high-energy charged particles were magnetically deflected out of their circular orbits in the 184-inch synchrocyclotron, and passed through a premagnet collimator, a steering magnet, and a collimator 1 inch in diameter by 48 inches long into the experimental area (cave). The full-energy beams were essentially monoenergetic, with a probable energy spread about the mean of less than 1%. To reduce the energy of the beam, internal absorbers were placed on a movable probe that could be positioned so that all the beam from the magnetic channel had to pass through these absorbers. Beryllium was used as the absorbing material in order that the multiple Coulomb scattering effects could be kept small, thus keeping the beam intensity as high as possible. The current to the focusing

Table I

Sample thicknesses and correction factors for fission loss due to self-absorption for samples used in the charged-particle bombardments

Sample	Thickness (mg/cm^2)	Sample Thickness Correction Factor
U^{238}	0.67	1.08 ± .03
U^{235} (95% pure)	0.811	1.10 ± .04
Th^{232}	1.13	1.14 ± .05
Bi	0.83	1.10 ± .04
Au	1.045	1.13 ± .04

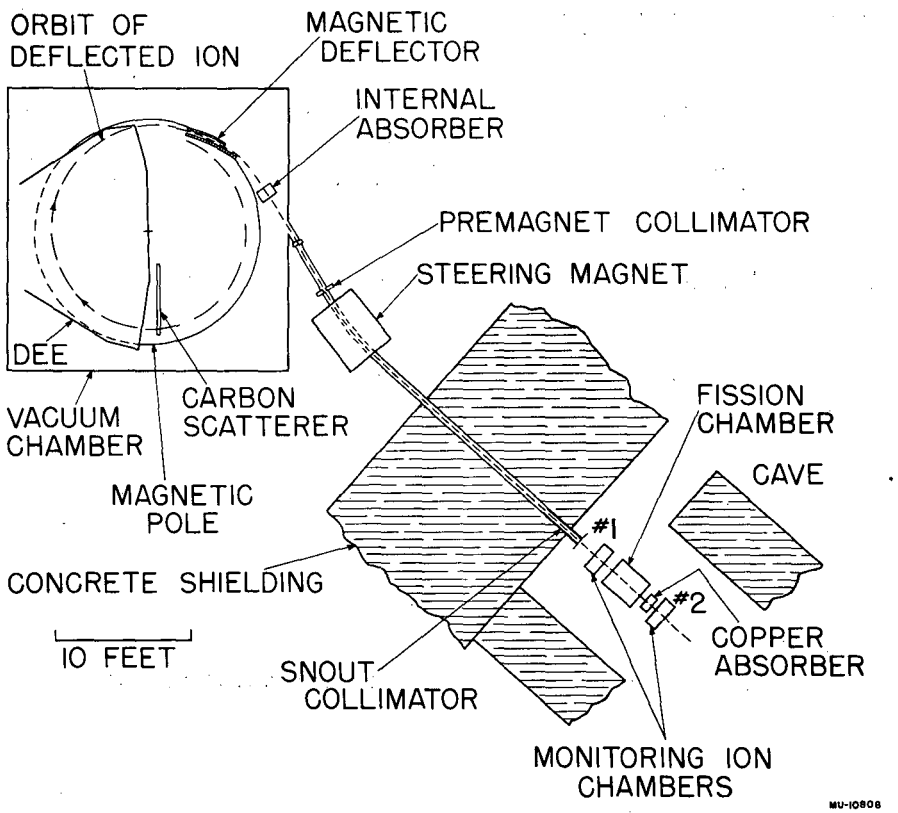

Fig. 5. Schematic diagram of the experimental arrangement at the cyclotron. (The representation of the experimental equipment in the cave is not to scale.)

magnet was then adjusted so as to guide the reduced-energy particles down the 48-inch collimator. The steering magnet also acted as momentum selector, and thus reduced the energy spread introduced by range straggling in the absorbers. Upon entering the cave the beam first passed through the monitoring ionization chamber (No. 1) and then through the fission chamber. The beam next passed through a variable copper absorber and finally through a second ionization chamber (No. 2). From the ratio of the charge collected in ion chamber No. 2 to the charge collected in ion chamber No. 1, with various amounts of copper absorber in between the chambers, a Bragg curve was obtained, and hence the energy of the beam could be determined.

B. Procedure

1. Alignment

The alignment of the fission chamber was checked with photographic film. These pictures were taken every time the current in the steering magnet was changed.

2. Variation of High Voltage on Electrodes B and C

Under usual operating conditions the high voltage on electrode B was + 1500 volts. If this voltage was changed to 1000 volts (with a simultaneous reduction of the voltage on electrode C, so that cancellation was maintained), the slope of the integral bias curve would increase; however, the extrapolated end point at zero bias would remain the same within statistics. Conversely, when the voltage on B was increased to + 2000 volts, the slope of the bias curve decreased but the end point was still unchanged. (Fig. 4). Unfortunately, when the voltage on electrode C was set at values above 4000 volts, occasional spark breakdowns occurred which registered as fission pulses. We therefore decided to operate electrodes B and C at + 1500 and + 3300 volts respectively.

3. Background and Cancellation

A periodic check was made of the cancellation and background by inserting a blank piece of 0.001-inch aluminum foil in place of the fissionable sample. Occasionally, pulses caused by the interaction of the beam with the aluminum sample backing or with the foil of the middle capacitor plate (plate B) would be counted by our electronic equipment. The number of these background beam pulses remained quite constant for a given beam intensity at a given energy, and thus could be subtracted with good reliability. Most of these pulses were quite small, and therefore they were counted mainly by the lowest biased scalers. The number of such background pulses detected by the lowest biased scaler was less than 1% of the number of fission pulses for U^{238}, U^{235}, and Th^{232}, less than 10% of the number of bismuth fission pulses, and less than 25% of the number of fission pulses from gold for all types of incident particles at all energies.

4. Pile-Up of Fission Pulses

The 184-inch synchrocyclotron has a repetition rate of 60 pulses per second. Each pulse of the scattered proton beam has a duration of about 20 microseconds, whereas for alpha particles and deuterons the pulse duration is about 40 μsec. These pulses have an rf fine structure; however, this fine structure is of no importance in this experiment, since the resolving time of the electronic equipment used in conjunction with the fission chamber was long (5μsec) compared to the characteristic time of the rf oscillations. In order to keep the loss of fission events due to pile-up of fission pulses to less than 1%, we chose the beam intensity so as to give less than 300 fission counts per minute for protons, and less than 500 fission counts per minute for alpha particles and deuterons. These limits on the counting rates were determined by making a curve of the counting rate per microcoulomb of charge collected on the beam monitoring ionization chamber, versus the reciprocal of the beam intensity. Such a curve is shown in Fig. 6.

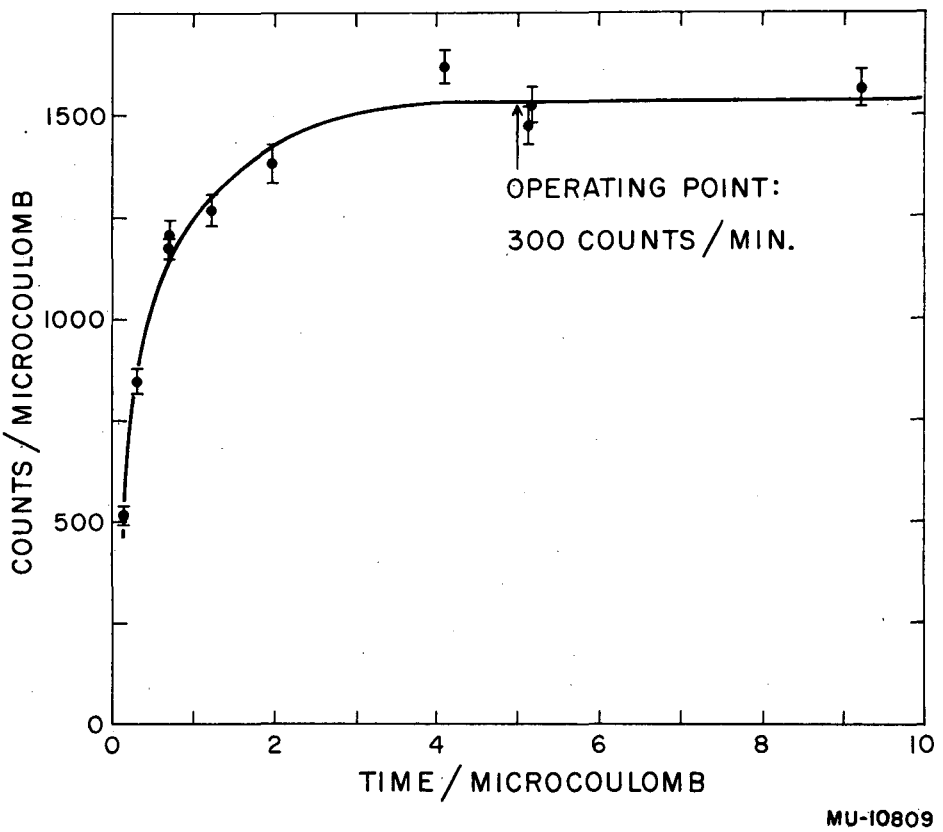

Fig. 6. Counting rate plotted against the reciprocal of the beam intensity. The ordinate shows the number of counts observed while the beam monitor collected 1 microcoulomb of charge. The abscissa shows the time (in minutes) necessary to charge the beam monitor to 1 microcoulomb.

No change was observed in either the total number of observed fission pulses or the shape of the bias curves when the clipping time of our amplifier was changed from 5 μsec to 1 μsec, if the amplifier gain was raised so as to keep the pulse height constant.

5. Gating of Scalers

In order to minimize the effects of pulses due to electrical disturbances in the cyclotron building, an electronic gate was employed that allowed the scalers to count only while the beam was on. This was helpful because occasionally electrical transients would cause spurious pulses to be detected during the 5-μsec resolving time of our electronics when the gate was not used. Since the beam-monitoring ionization chambers were not gated, it was important to make sure that no fission counts were being lost because of the gating procedure. To do this the gating circuit was switched so as to allow the scalers to count only during the time that the beam was not on. No counts above background were observed.

6. Geometry of the Fission Chamber

The geometry of the fission chamber was tested by placing an alpha standard in place of one of the fissionable samples on the ladder-shaped frame in the chamber. The diameter of the alpha standard was about 1.25 inches, which was approximately equal to the beam size at the targets when the chamber was used at the cyclotron. Upon comparison of the counting rate of the alpha standard as measured in the fission chamber with the counting rate as measured in an ionization chamber whose geometry was strictly that of flat parallel plates, it was found that 1.5 ± 0.5% fewer counts were observed in the fission chamber. This is presumable because the ladder-shaped frame would position the sample approximately 1/32 inch behind electrode A. Hence, the effective solid angle was slightly less than 2π steradians.

7. Neutrons

The neutron contamination of each beam was checked by placing sufficient copper absorber to completely stop the beam immediately in front of the fission chamber. This check probably overestimated the neutron contamination, because of the additional neutrons produced by the charged particles in the copper absorber. In any case the fissioning effect of these neutrons was less than 1% of the charged-particle-induced fission rate for all samples except U^{235}. For U^{235} this effect was approximately 2%.

8. Momentum Transfer to Struck Nucleus

The usual orientation of the fission chamber was chosen in such a way that the fission fragments were observed in the backward hemisphere with respect to the beam direction. Since a fission fragment is a rather slowly moving object (e.g., an 80-Mev fission fragment of $A = 100$ has $\beta = 0.04$, where β is the velocity of the fragment divided by the velocity of light), a small amount of momentum transferred to the target nucleus appreciably distorts the angular distribution of the fission fragments in the laboratory system. For example, if a 340-Mev proton were to transfer all of its momentum to a target nucleus of U^{238}, then the target nucleus, which is the center-of-mass frame for the fission fragments, would have $\beta = 0.0039$. If we assume (a) that the fission fragments are emitted isotropically in their center-of-mass system, and (b) that we have a thin sample, then the motion of the fissioning nucleus would cause about 10% fewer fragments to enter the sensitive region of the ionization chamber than when the fission occurs with the nucleus at rest. In other words the center-of-mass motion causes the effective solid angle available to the detected fission fragments to be reduced by 10%, when the beam passes through the chamber in the direction CBA. On the other hand, if the orientation of the chamber is ABC with respect to the beam direction, 10% more fragments enter the sensitive region of the ionization chamber. However, in the second case no increase in the counting rate is observed, since only one pulse is detected, whether it is caused by only one fragment or by both fragments emitted simultaneously.

If (a) we have a sample of finite thickness in which a fraction η of the fragments is self-absorbed when the fission occurs with the nucleus at rest, and if (b) there is a fractional change ξ in the effective solid angle due to the center-of-mass motion, then if the beam direction is CBA the fraction of the fissions observed in our chamber is $1-\eta-\xi$. On the other hand, if the beam direction is ABC, this fraction is approximately $1 - \eta + \xi - \frac{\xi^2}{4\eta}$ for $0 < \xi < 2\eta$, and 1 for $\xi > 2\eta$. In this experiment we had $\xi < 2\eta$ in all cases. Hence, by taking the ratio of the fissions observed when the chamber is oriented in the direction ABC, we can determine ξ; i.e.,

$$\frac{\text{CBA}}{\text{ABC}} = 1 - 2\xi + \frac{\xi^2}{4\eta} .$$

Since $\xi \cong \frac{\beta \text{ (target nucleus)}}{\beta \text{ (fission fragment)}}$, the ratio $\frac{\text{CBA}}{\text{ABC}}$ yields a value for the amount of momentum transferred to the fissioning nucleus by the incident particle. These data are summarized in Table II. Furthermore, the knowledge of the amount of momentum transferred to the target nucleus allows us to make a crude estimate of the excitation energy of the struck nucleus. To do this let us envisage the collision process as follows: (1) The incident particle collides with one or more nucleons in the nucleus. (2) As a result of the collision n cascade nucleons are emitted. These cascade nucleons will be emitted primarily in the forward direction. (3) The excited nucleus has several ways to rid itself of its excess energy. For the purpose of this discussion we will consider only (a) evaporation of nucleons, and (b) fission. The following equations express the conservation of energy and momentum in this process:

$$E_0 + Mc^2 = M' c^2 + \sum_{i=1}^{n} E_i + E_e ,$$

$$\vec{p}_0 = \sum_{i=1}^{n} \vec{p}_i + \vec{P} ,$$

Table II

Momentum transfer to struck nucleus

Sample	Energy (Mev)	$\frac{CBA}{ABC}$	r	η	ξ	ξ_{max}	$\alpha = \frac{\Delta p}{p}$
Bombarding Particles:		Protons					
U^{238}	336	0.933	0.067 ± .035	0.08 ± .03	0.0353 ± .018	0.097	0.36 ± .19
U^{235}		0.918	0.082 ± .032	0.10 ± .04	0.0432 ± .016	0.099	0.44 ± .16
Th		0.941	0.059 ± .034	0.14 ± .05	0.0303 ± .017	0.100	0.30 ± .17
Bi		0.871	0.129 ± .034	0.10 ± .04	0.0700 ± .017	0.110	0.64 ± .15
U^{238}	190	0.976	0.024 ± .041	0.08 ± .03	0.0122 ± .022	0.070	0.17 ± .1
U^{235}		0.979	0.021 ± .037	0.10 ± .04	0.0107 ± .019	0.071	0.15 ± .2
Th		0.926	0.074 ± .040	0.14 ± .05	0.0383 ± .020	0.072	0.53 ± .28
Bi		0.863	0.137 ± .103	0.10 ± .04	0.0744 ± .052	0.080	0.93 ± .65
Bombarding Particles:		Alpha Particles					
U^{238}	375	0.866	0.134 ± .037	0.08 ± .03	0.0740 ± .019	0.193	0.38 ± .10
U^{235}		0.848	0.152 ± .034	0.10 ± .04	0.0833 ± .017	0.195	0.43 ± .09
Th		0.867	0.133 ± .035	0.14 ± .05	0.0705 ± .018	0.198	0.36 ± .09
Bi		0.868	0.132 ± .043	0.10 ± .04	0.0715 ± .022	0.220	0.33 ± .10
U^{238}	240	0.839	0.161 ± .049	0.08 ± .03	0.0906 ± .025	0.152	0.60 ± .16
U^{235}		0.877	0.123 ± .045	0.10 ± .04	0.0662 ± .023	0.155	0.43 ± .15
Th		0.832	0.168 ± .045	0.14 ± .05	0.0904 ± .023	0.158	0.57 ± .15

$r = 1 - \frac{CBA}{ABC}$

To calculate α it was assumed that all fission fragments have a velocity of $\beta = 0.04$.

where E_0 = total energy of incident particle (kinetic energy + rest energy),

M = mass of target nucleus,

M' = mass of excited nucleus after the cascade process, but before evaporation of nucleons,

E_i = total energy of ith cascade particle,

E_e = excitation energy of struck nucleus after cascade process, but before evaporation,

$\vec{p}_0$ = momentum of incident particle,

$\vec{p}_i$ = momentum of ith cascade nucleon,

$\vec{P}$ = momentum of fissioning nucleus before the evaporation of nucleons or fission.

If we now assume that

(1) the evaporated nucleons are emitted isotropically from the excited nucleus, and

(2) only one cascade nucleon is emitted (i.e., $n = 1$) at an angle θ (with respect to the incident beam direction),

then $E_0 + Mc^2 = M'c^2 + E_1 + E_e$.

Further, if the incident particle was a proton, then

$$E_0 = E_1 + E_e$$

and

$$p_0 = p_1 \cos\theta + P \cos\phi ;$$

where ϕ = angle of fissioning nucleus with respect to the beam direction;

$$\therefore E_e = E_0 - E_1$$

$$= E_0 - \sqrt{p_1^2 c^2 + M^2 c^4},$$

$P \cos\phi = \Delta p$ (= observed momentum transfer along the beam direction)

$$= a\, p_0;$$

$$\therefore p_0 = p_1 \cos\theta + a\, p_0$$

or

$$p_1 = \frac{(1 - a)}{\cos \theta} p_0 ,$$

and

$$E_e = E_0 - \sqrt{\frac{(1 - a)^2}{\cos^2 \theta} p_0^2 c^2 + M^2 c^4} .$$

Recalling that

$$E_0 = \sqrt{p_0^2 c^2 + M^2 c^4},$$

we have

$$E_e = E_0 \left[1 - \frac{1}{\gamma} \sqrt{\frac{(1 - a)^2 (\gamma^2 - 1)}{\cos^2 \theta} + 1} \right]$$

where

$$\gamma = \frac{E_0}{Mc^2} .$$

In Table III we have calculated E_e for $\theta = 0^o$ and $\theta = 30^o$.

Table III

Excitation Energy of Struck Nucleus			
Sample	Proton Kinetic Energy (Mev)	E_e (0^o) (Mev)	E_e (30^o) (Mev)
U^{238}	336	184 ± 83	140 ± 107
U^{235}	336	219 ± 64	182 ± 82
Th^{232}	336	158 ± 79	107 ± 101
Bi^{209}	336	292 ± 41	276 ± 53
U^{238}	192	55 ± 94	15 ± 125
U^{235}	192	38 ± 83	4.5 ± 110
Th^{232}	192	145 ± 53	131 ± 70
Bi^{209}	192	191 ± 19	191 ± 25

IV. RESULTS

The fission cross sections of U^{238}, U^{235}, Th^{232}, Bi^{209}, and Au^{197} for protons, deuterons, and alpha particles are presented in TablesIV to VI and plotted in Figs. 7 through 21. Only standard deviations due to counting statistics are indicated on the graphs. In addition to the statistical errors the following systematic errors may be ascribed to the experiment: (a) determination of sample thickness, ± 3%; (c) self-absorption of fission fragments in the sample material, ± 5%; (d) extrapolation to zero bias, ± 5%; (e) momentum transfer to the target nucleus, ± 1.5%; (f) determination of beam energy, ± 1%; (g) calibration of beam monitor, ± 3%; (h) geometry of the chamber, ± 0.5%. When these errors are compounded, a total systematic error of 9% may be ascribed to the experiment. The accuracy of the absolute cross sections may be obtained by combining the above systematic errors with the errors due to counting statistics shown in Figs. 7 through 21.

Table IV

Proton-induced fission cross sections
(In Units of 10^{-24} cm^2)

E_p (Mev)	U^{238}	U^{235}	Th^{232}	Bi^{209}	Au^{197}
336	1.35 ± .01	1.30 ± .01	0.82 ± .01	0.198 ± .002	0.051 ± .001
302	1.38 ± .03	1.35 ± .02	0.79 ± .02	0.188 ± .006	0.040 ± .001
287	1.37 ± .03	1.30 ± .03	0.81 ± .02	0.203 ± .008	0.051 ± .004
261	1.34 ± .02	1.36 ± .02	0.81 ± .02	0.191 ± .005	0.038 ± .002
253	1.33 ± .04	1.33 ± .04	0.80 ± .02	0.175 ± .005	0.036 ± .002
230	1.32 ± .02	1.30 ± .02	0.80 ± .02	0.157 ± .004	0.038 ± .001
216	1.31 ± .03	1.28 ± .03	0.82 ± .02	0.173 ± .005	0.038 ± .002
193	1.35 ± .05	1.33 ± .04	- -	- -	- -
191	1.38 ± .02	1.34 ± .03	0.85 ± .02	0.148 ± .009	- -
182	1.36 ± .04	1.32 ± .04	0.87 ± .03	0.147 ± .011	0.028 ± .006
177	1.30 ± .03	1.36 ± .03	0.86 ± .02	0.155 ± .005	0.032 ± .002
158	1.47 ± .06	1.36 ± .06	0.90 ± .03	0.146 ± .008	0.016 ± .007
153	1.43 ± .05	1.52 ± .04	0.96 ± .03	0.136 ± .008	- -
132	1.35 ± .05	1.52 ± .04	0.90 ± .03	0.125 ± .008	0.017 ± .003
130	1.33 ± .05	1.20 ± .04	0.88 ± .03	- -	- -
114	1.37 ± .15	1.68 ± .17	0.89 ± .09	- -	- -

Table V

Deuteron-induced fission cross sections
(In Units of 10^{-24} cm^2)

E_d (Mev)	U^{238}	U^{235}	Th^{232}	Bi^{209}	Au^{197}
192	- -	2.01 ± .03	- -	- -	- -
190	1.98 ± .05	1.94 ± .05	1.28 ± .02	0.245 ± .005	0.055 ± .002
187	2.24 ± .04	2.24 ± .05	1.46 ± .03	0.249 ± .009	0.054 ± .002
159	1.98 ± .05	1.90 ± .05	1.22 ± .03	0.198 ± .006	0.037 ± .003
143	2.10 ± .04	2.06 ± .03	1.32 ± .03	0.207 ± .004	0.040 ± .002
118	2.01 ± .04	2.08 ± .04	1.35 ± .03	0.192 ± .012	- -
118	- -	2.00 ± .05	- -	- -	- -
100	2.05 ± .04	2.00 ± .04	1.32 ± .03	0.143 ± .013	- -
93	2.46 ± .07	2.53 ± .05	1.55 ± .04	- -	- -
88	1.84 ± .05	1.90 ± .05	1.23 ± .03	0.096 ± .009	0.010 ± .005

Table VI

Alpha-particle-induced fission cross sections
(In Units of 10^{-24} cm^2)

Ea	U^{238}	U^{235}	Th^{232}	Bi^{209}	Au^{197}
380	2.18 ± .03	2.19 ± .03	1.56 ± .02	0.619 ± .010	0.191 ± .005
379	- -	2.33 ± .04	- -	- -	- -
376	2.34 ± .04	2.38 ± .04	1.565± .03	0.605 ± .016	0.187 ± .004
372	- -	2.24 ± .04	- -	- -	0.205 ± .006
370	2.36 ± .02	2.27 ± .02	1.60 ± .02	0.616 ± .007	0.189 ± .005
330	2.38 ± .05	2.21 ± .05	1.54 ± .03	0.666 ± .018	0.239 ± .009
309	- -	2.12 ± .05	- -	- -	- -
309	- -	2.28 ± .05	- -	- -	- -
300	2.19 ± .05	2.08 ± .05	1.49 ± .04	0.605 ± .016	0.197 ± .009
274	2.08 ± .05	2.00 ± .07	1.495± .04	0.588 ± .023	- -
252	2.35 ± .08	2.49 ± .08	1.74 ± .05	0.759 ± .033	0.244 ± .023
243	- -	2.42 ± .05	- -	- -	- -
242	- -	2.05 ± .11	- -	- -	- -
240	2.65 ± .10	2.01 ± .10	1.73 ± .07	0.850 ± .050	- -
239	2.22 ± .05	2.26 ± .05	1.515± .04	0.665 ± .025	0.214 ± .026
238	2.62 ± .10	2.40 ± .09	1.89 ± .07	- -	- -
238	2.33 ± .09	2.32 ± .08	1.675± .06	- -	- -
212	2.40 ± .10	2.22 ± .09	1.89 ± .07	0.690 ± .049	0.236 ± .034

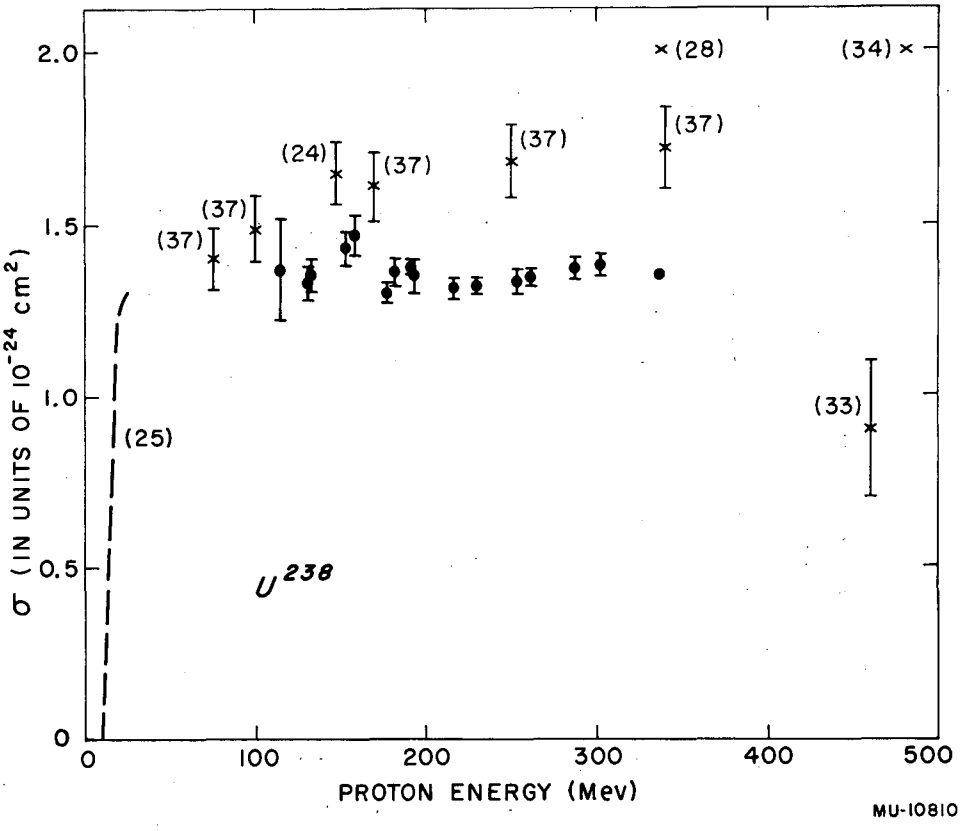

Fig. 7. Fission cross section of U^{238} as a function of proton energy. The results of this experiment are indicated by the circles, • . The errors indicated on these points are standard deviations due to counting statistics only. The results of other workers are indicated by numbers: (24), Harding, Reference 24; (25), McCormick and Cohen, Reference 25; (28), Folger, Stevenson, and Seaborg, Reference 28; (33), Perfilov, Ivanova, Lozhkin, Ostroumov, and Shamov, Reference 33; (35), Vinogradov, Alimarin, Baranov, Lavrukhina, Baranova, Pavlotskaya, Bragina, and Yakovlev, Reference 35; (38), Hicks and Gilbert, Reference 38.

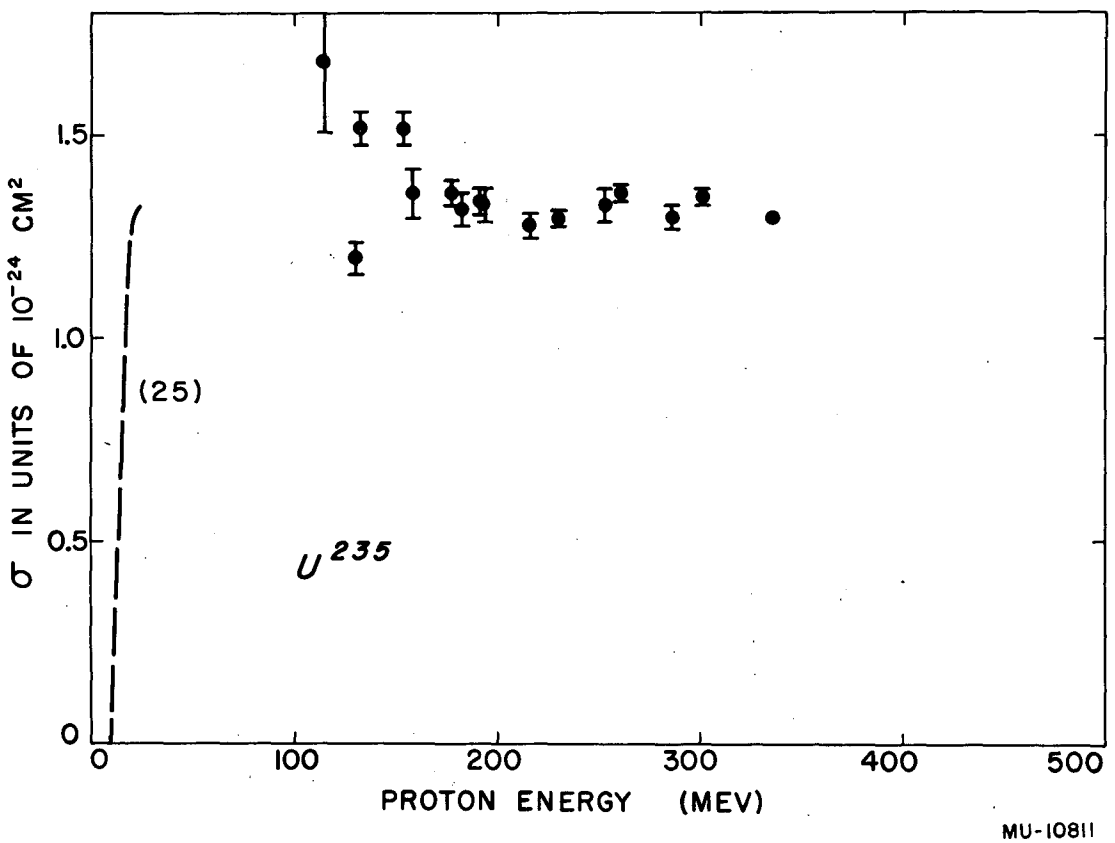

Fig. 8. Fission cross section of U^{235} as a function of proton energy. The results of this experiment are indicated by the circles, •. The errors indicated on these points are standard deviations due to counting statistics only. The results of other workers are indicated by numbers: (25), McCormick and Cohen, Reference 25.

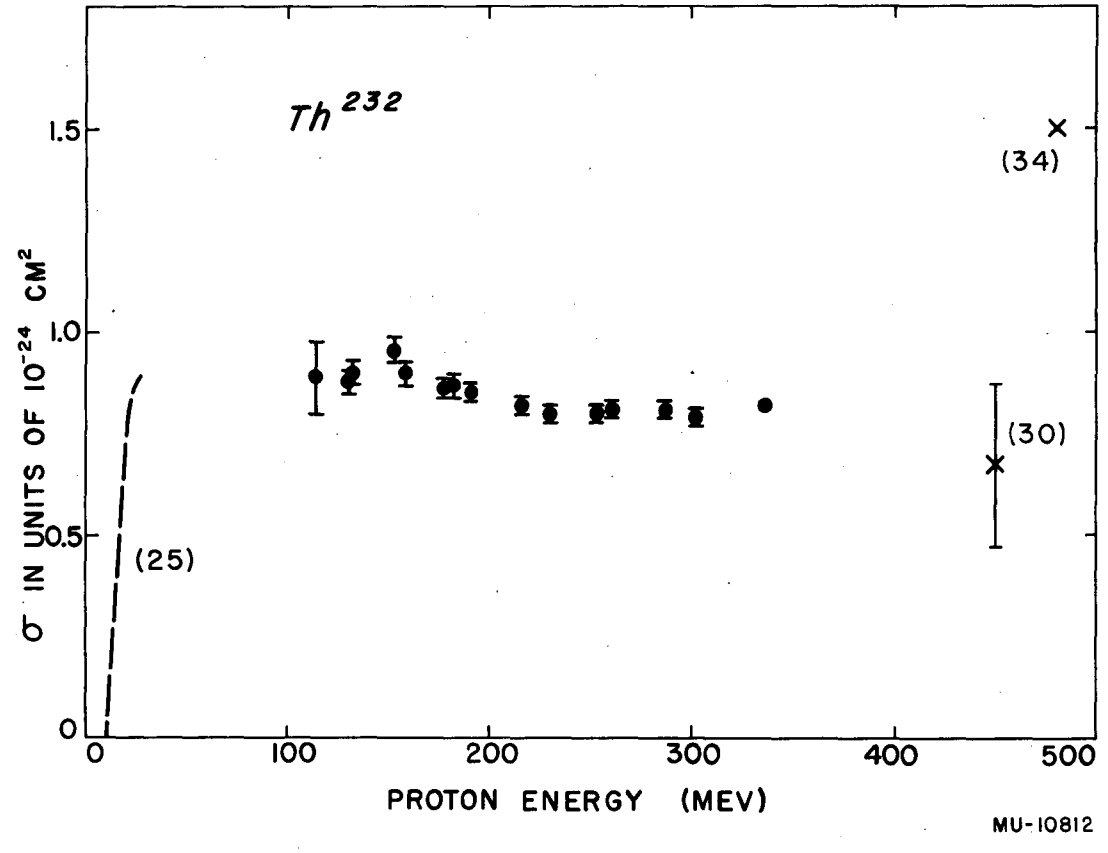

Fig. 9. Fission cross section of Th^{232} as a function of proton energy. The results of this experiment are indicated by the circles, •. The errors indicated on these points are standard deviations due to counting statistics only. The results of other workers are indicated by numbers: (25), McCormick and Cohen, Reference 25; (30), Kruger and Sugarman, Reference 30; (35), Vinogradov, Alimarin, Baranov, Lavrukhina, Baranova, Pavlotskaya, Bragina, and Yakovlev, Reference 35.

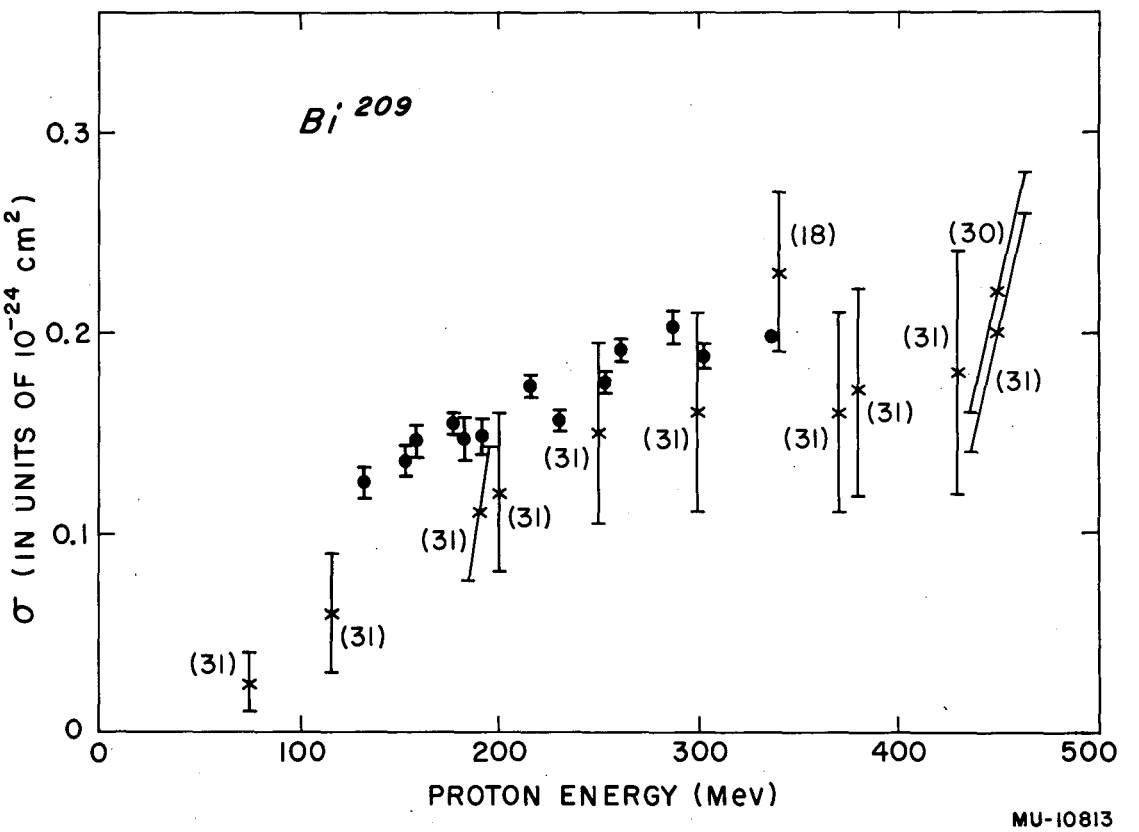

Fig. 10. Fission cross section of Bi^{209} as a function of proton energy. The results of this experiment are indicated by the circles, ● . The errors indicated on these points are standard deviations due to counting statistics only. The results of other workers are indicated by numbers: (18), Biller, Reference 18; (30), Kruger and Sugarman, Reference 30; (31) Jodra and Sugarman, Reference 31.

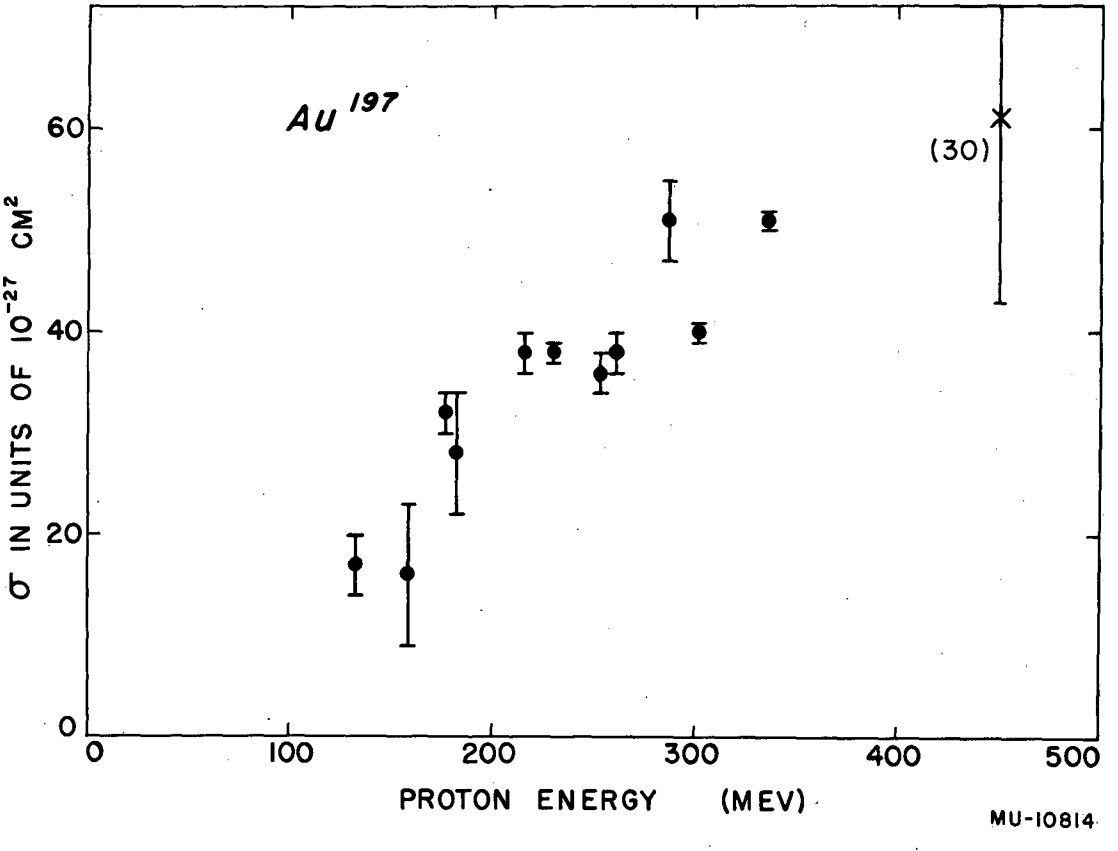

Fig. 11. Fission cross section of Au^{197} as a function of proton energy. The results of this experiment are indicated by the circles, •. The errors indicated on these points are standard deviations due to counting statistics only. The results of other workers are indicated by numbers: (30), Kruger and Sugarman, Reference 30.

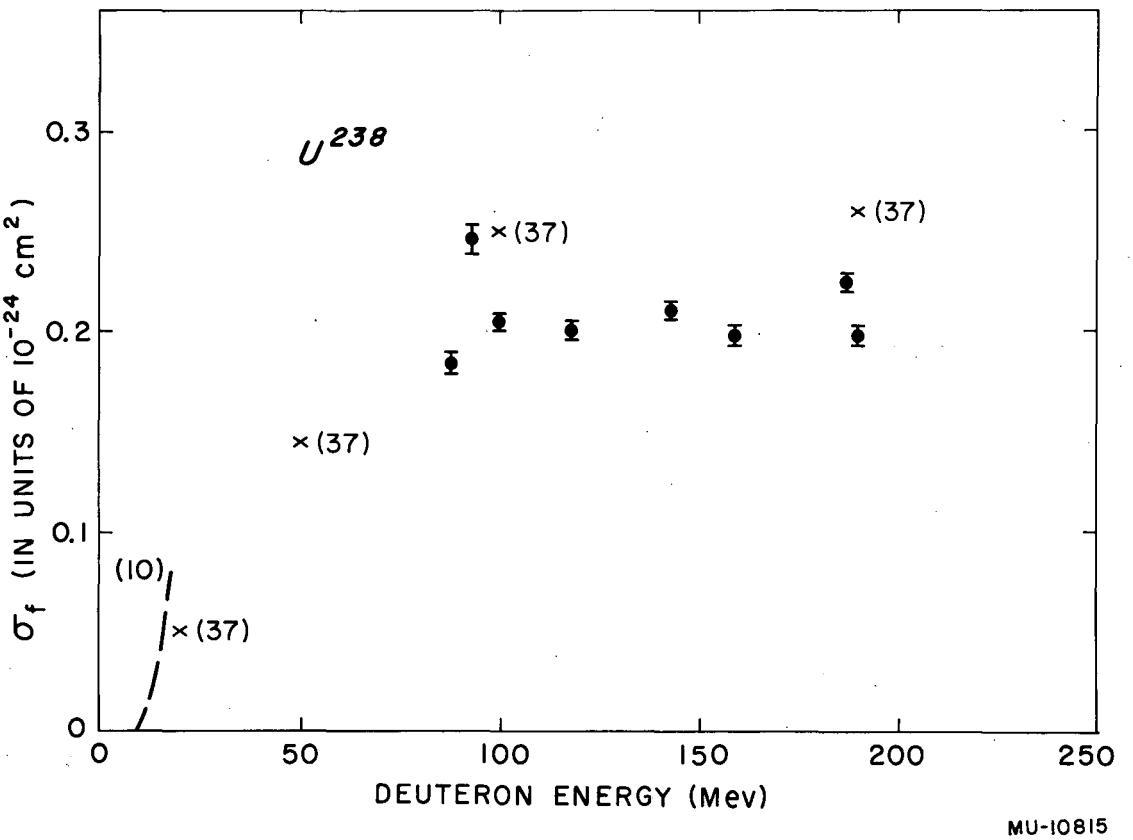

Fig. 12. Fission cross section of U^{238} as a function of deuteron energy. The results of this experiment are indicated by the circles, • . The errors indicated on these points are standard deviations due to counting statistics only. The results of other workers are indicated by numbers: (10), Jungerman, Reference 10; (38), Hicks and Gilbert, Reference 38.

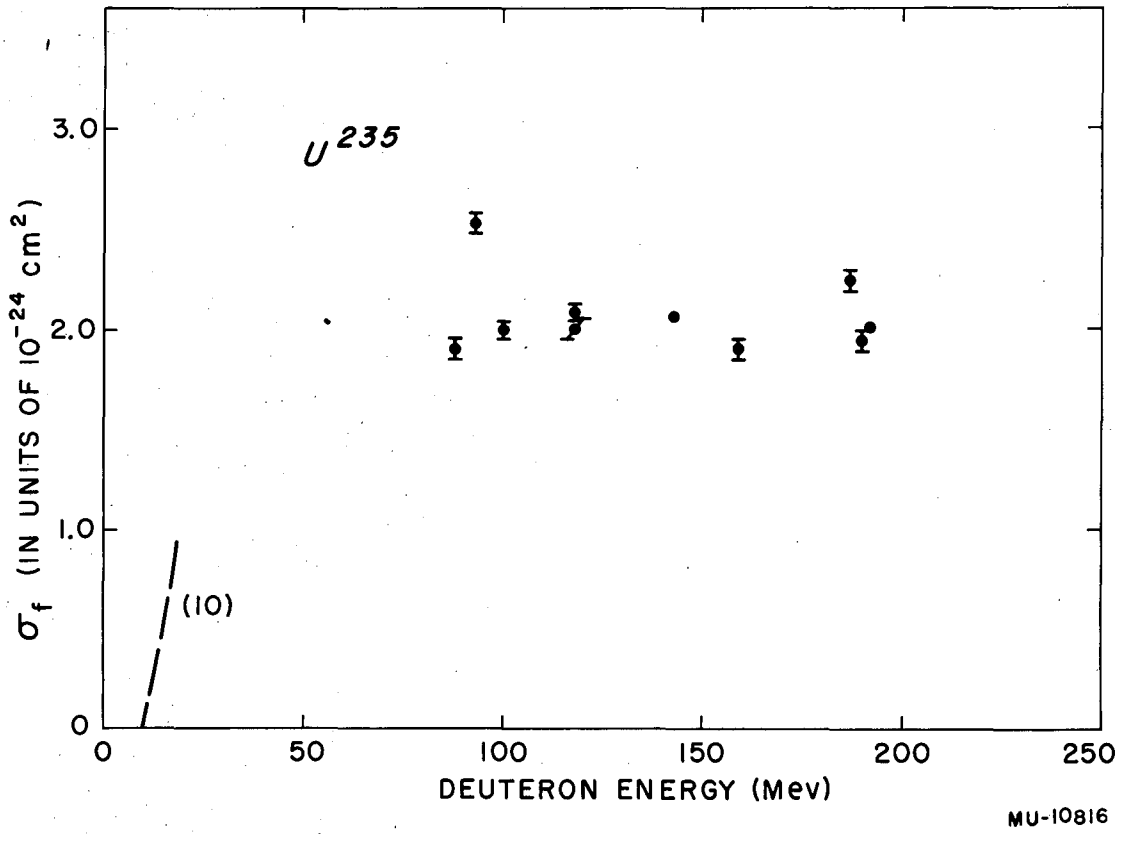

Fig. 13. Fission cross section of U^{235} as a function of deuteron energy. The results of this experiment are indicated by the circles, ● . The errors indicated on these points are standard deviations due to counting statistics only. The results of other workers are indicated by numbers: (10), Jungerman, Reference 10.

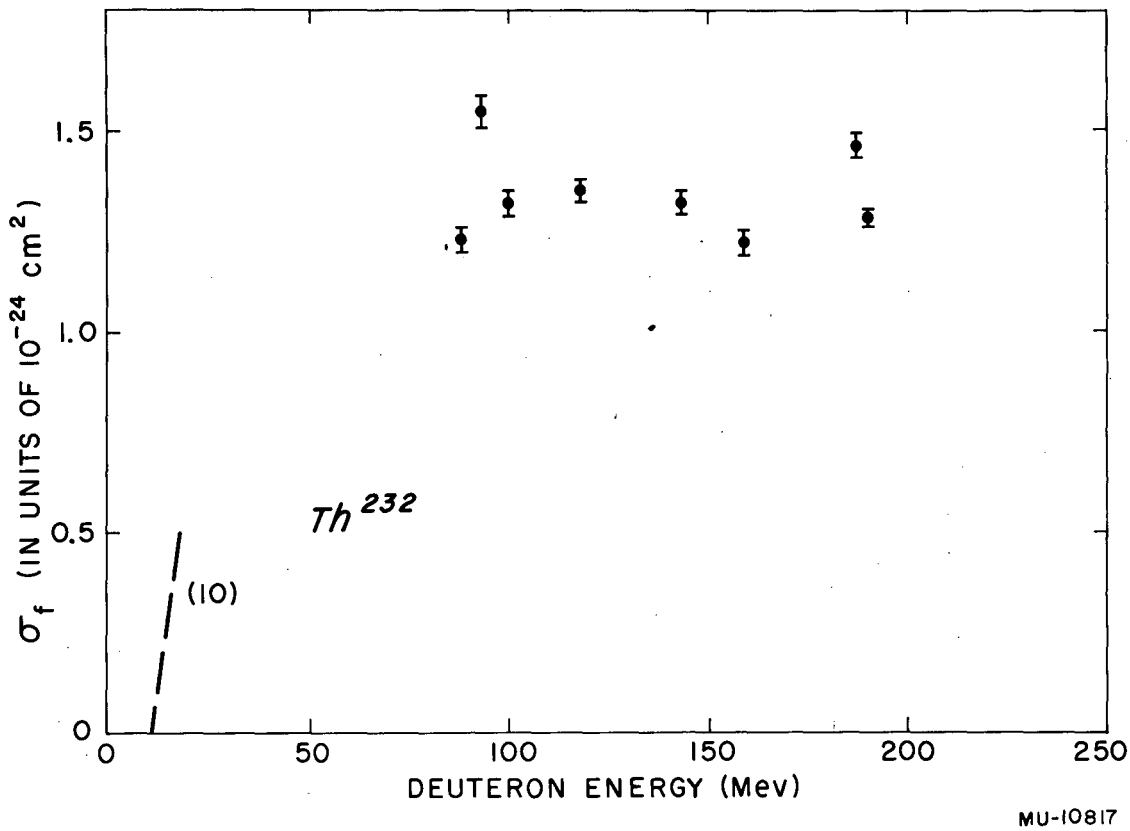

Fig. 14. Fission cross section of Th^{232} as a function of deuteron energy. The results of this experiment are indicated by the circles, • . The errors indicated on these points are standard deviations due to counting statistics only. The results of other workers are indicated by numbers: (10), Jungerman, Reference 10.

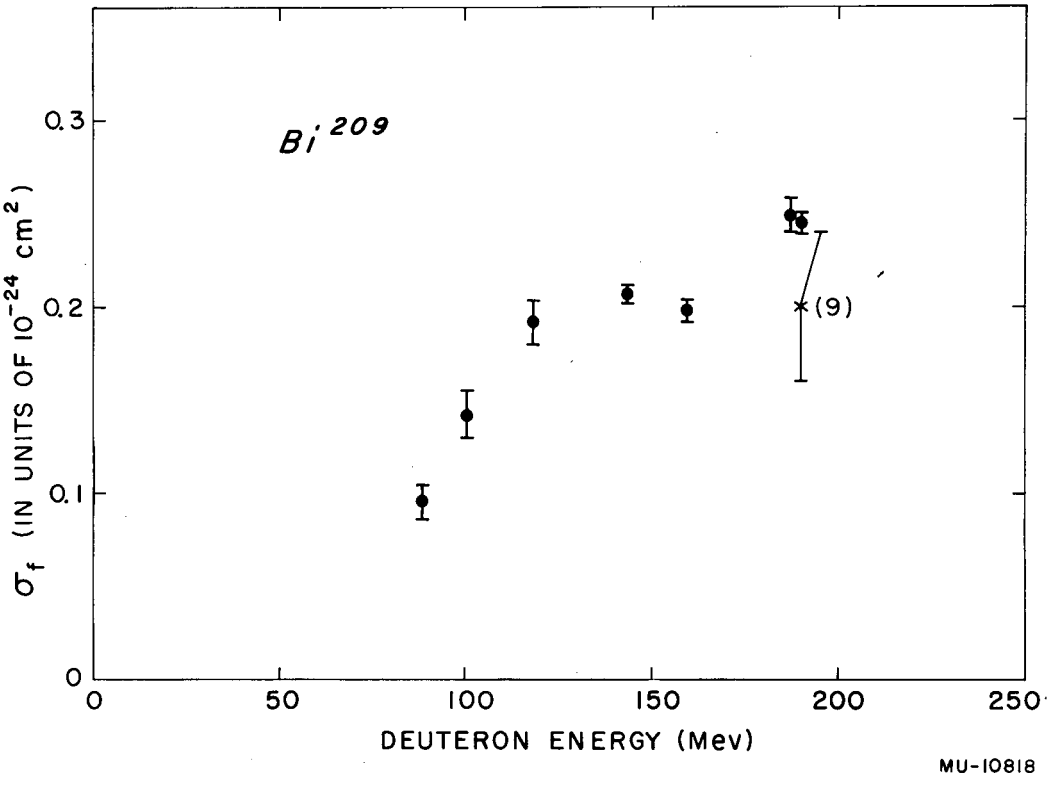

Fig. 15. Fission cross section of Bi^{209} as a function of deuteron energy. The results of this experiment are indicated by the circles, ● . The errors indicated on these points are standard deviations due to counting statistics only. The results of other workers are indicated by numbers: (9), Goeckerman and Perlman, Reference 9.

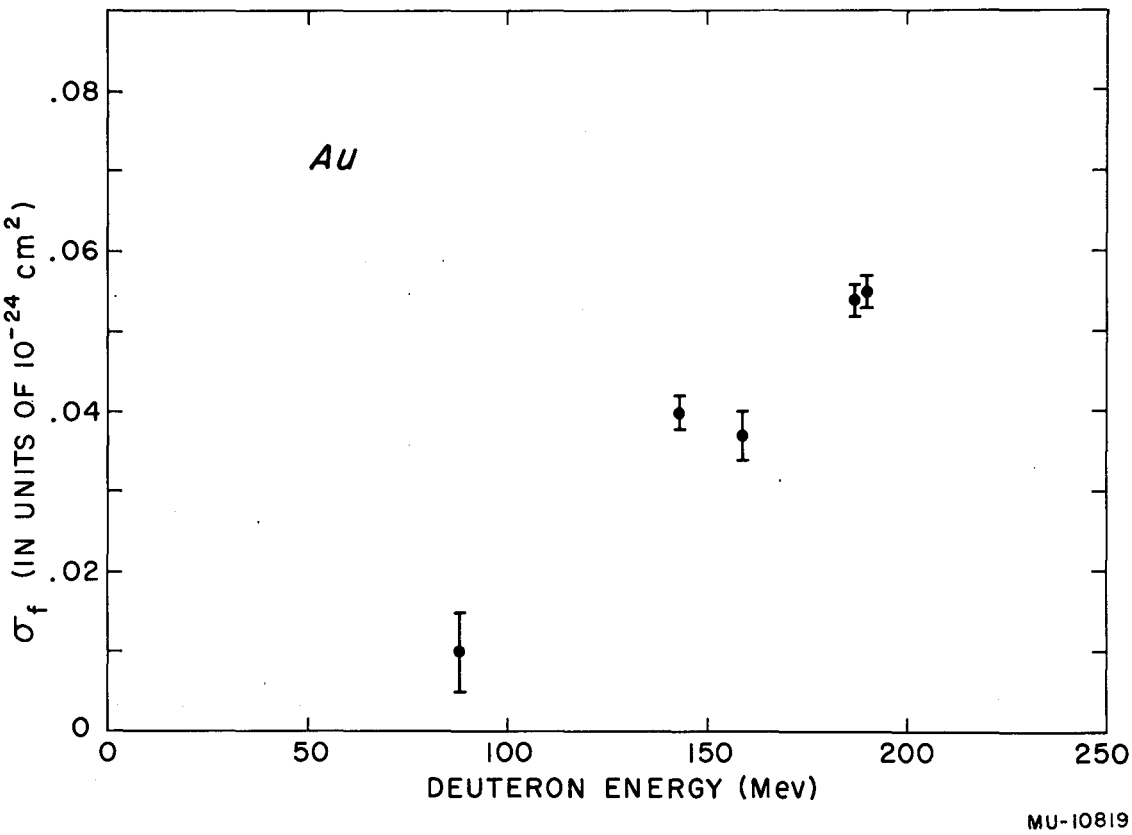

Fig. 16. Fission cross section of Au^{197} as a function of deuteron energy. The results of this experiment are indicated by the circles, ⊙ . The errors indicated on these points are standard deviations due to counting statistics only.

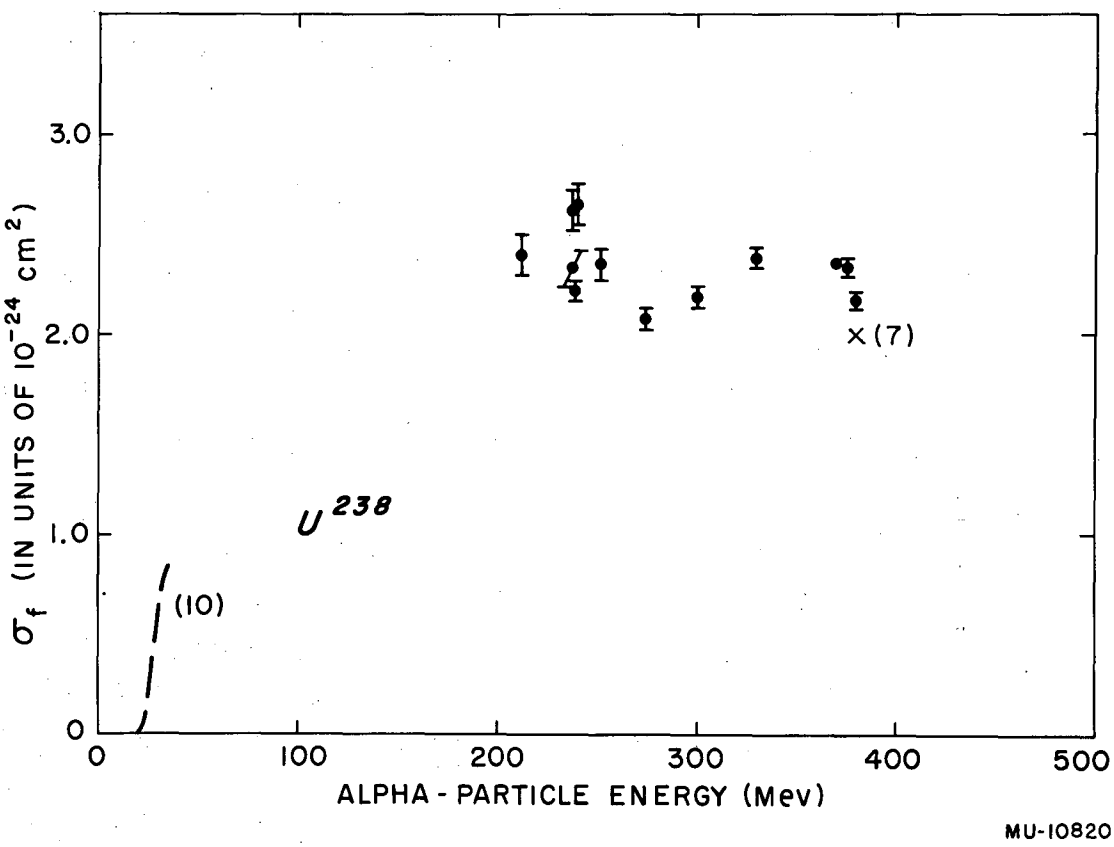

Fig. 17. Fission cross section of U^{238} as a function of alpha-particle energy. The results of this experiment are indicated by the circles, ● . The errors indicated on these points are standard deviations due to counting statistics only. The results of other workers are indicated by numbers: (7), O'Connor and Seaborg, Reference 7; (10), Jungerman, Reference 10.

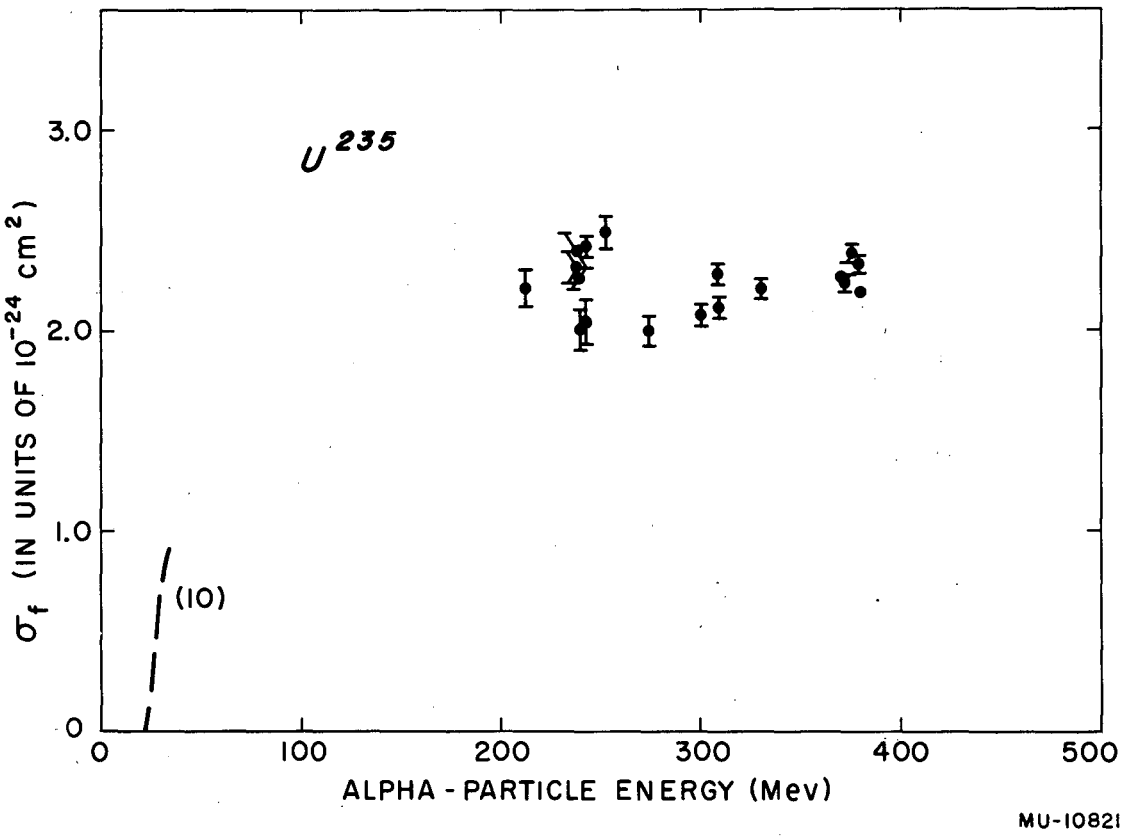

Fig. 18. Fission cross section of U^{235} as a function of alpha-particle energy. The results of this experiment are indicated by the circles, ● . The errors indicated on these points are standard deviations due to counting statistics only. The results of other workers are indicated by numbers: (10), Jungerman, Reference 10.

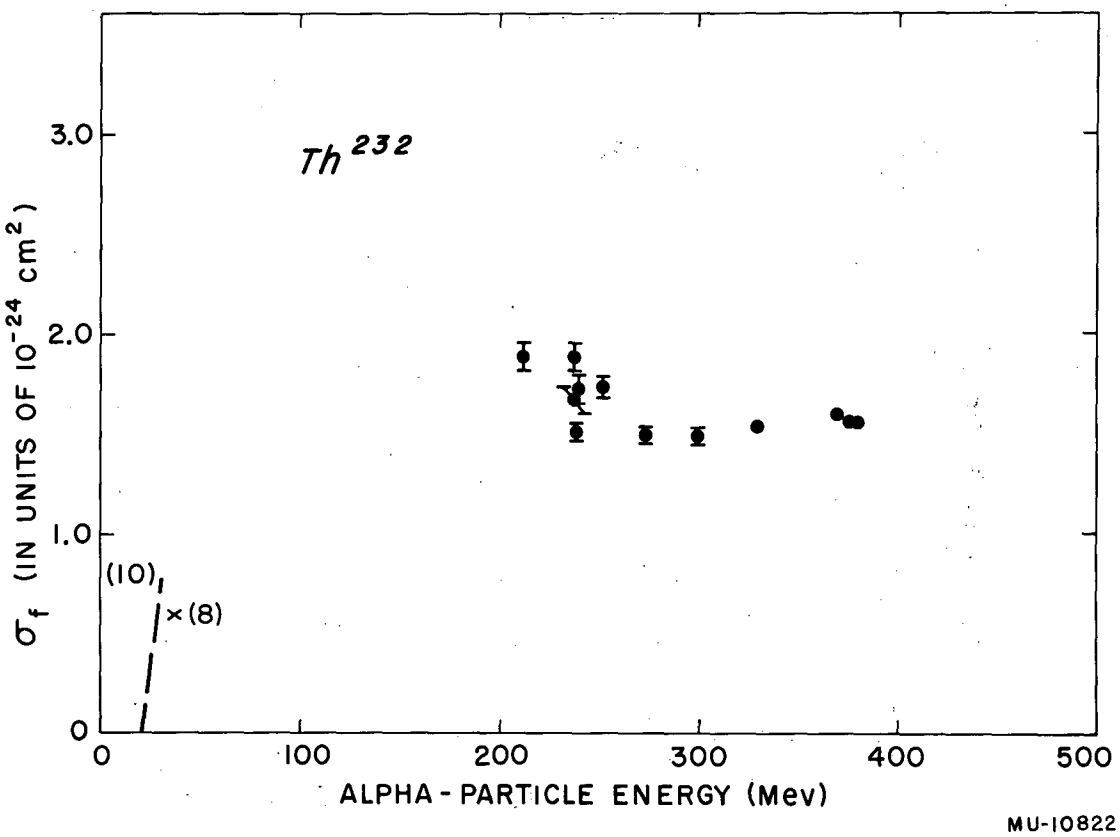

Fig. 19. Fission cross section of Th^{232} as a function of alpha-particle energy. The results of this experiment are indicated by the circles, • . The errors indicated on these points are standard deviations due to counting statistics only. The results of other workers are indicated by numbers: (8), Newton, Reference 8; (10), Jungerman, Reference 10.

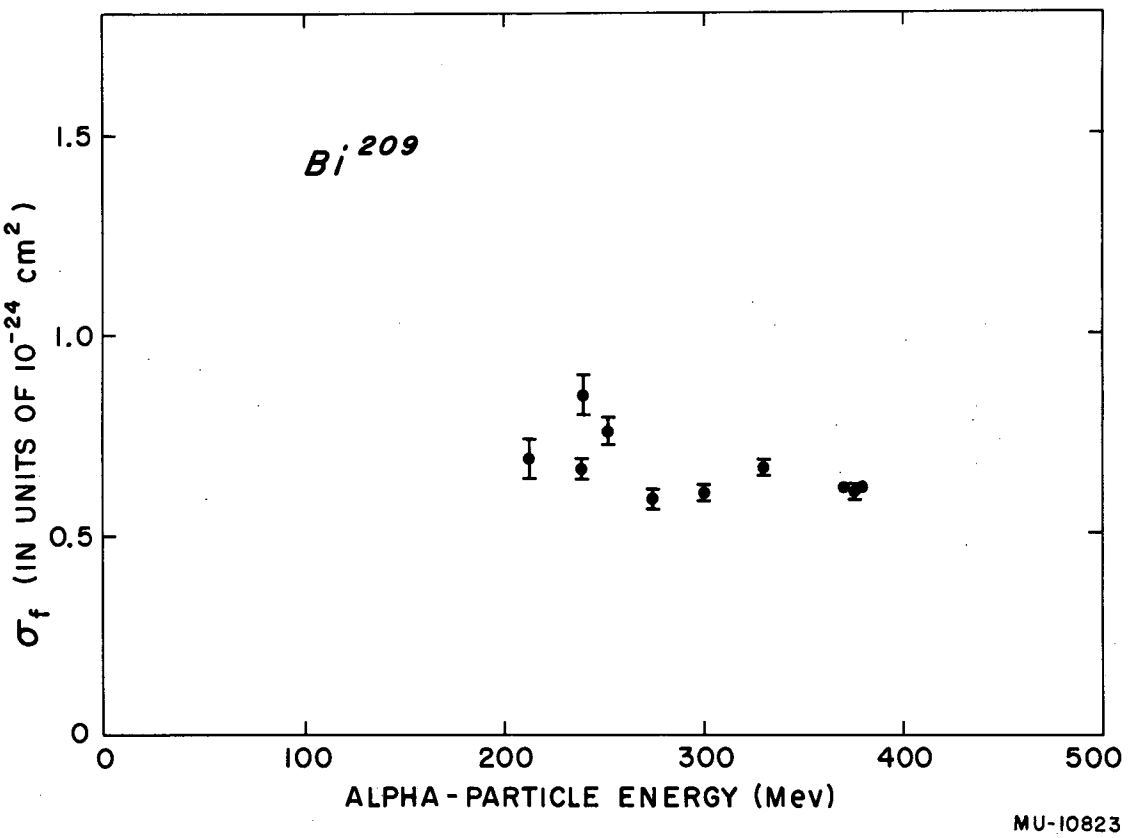

Fig. 20. Fission cross section of Bi^{209} as a function of alpha-particle energy. The results of this experiment are indicated by the circles, • . The errors indicated on these points are standard deviations due to counting statistics only.

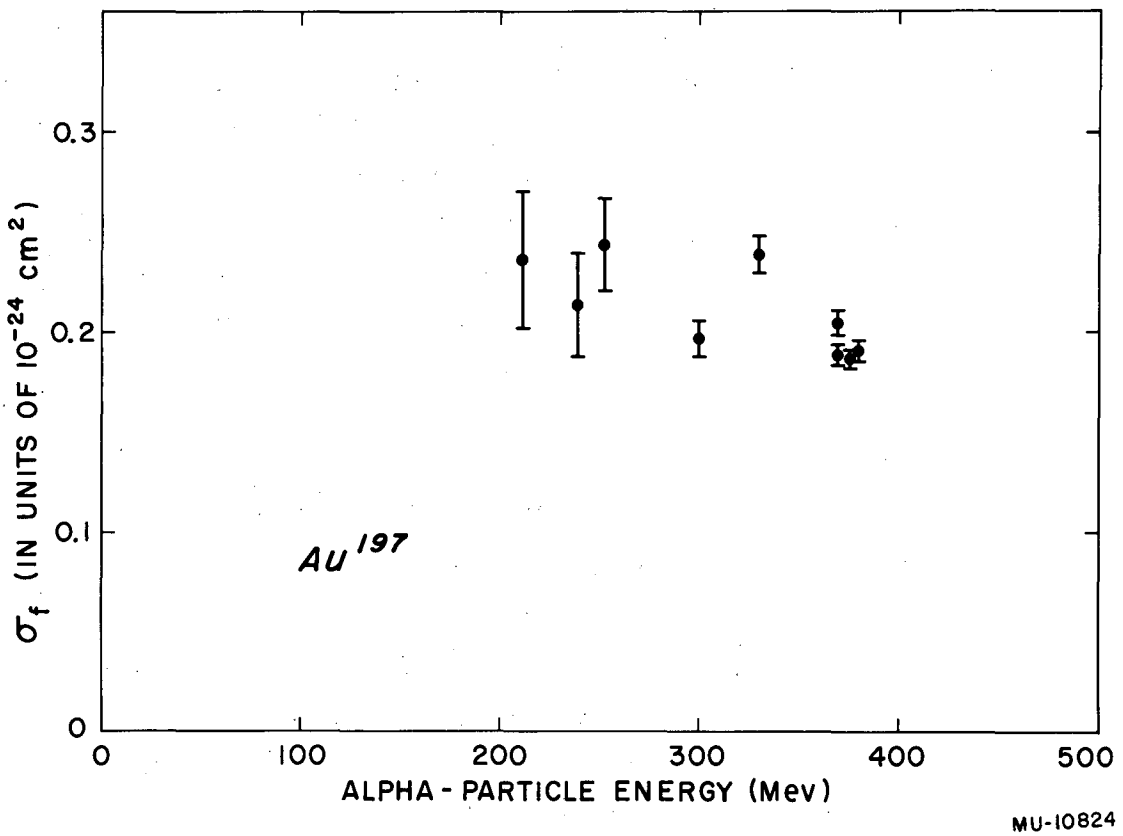

Fig. 21. Fission cross section of Au^{197} as a function of alpha-particle energy. The results of this experiment are indicated by the circles, ● . The errors indicated on these points are standard deviations due to counting statistics only.

V. DISCUSSION

A. Energy Dependence of Fission Cross Sections

One striking feature of the results of this experiment is the constancy of the fission cross sections of U^{238}, U^{235}, and Th^{232} as a function of the energy of the bombarding protons, deuterons, and alpha particles. The slight decrease in the proton-induced cross sections of U^{238}, U^{235}, and Th^{232} can be most easily explained if we recall that according to the optical model of the nucleus the transparency of the nucleus increases as the energy of the bombarding particles increases.[45] The cross sections of bismuth and gold, on the other hand, increase with increasing energy for protons and deuterons. Upon extrapolating the excitation functions for these samples to the point where the fission cross sections are greater than about 10^{-27} cm^2, we find "energy thresholds" of about 50 to 60 Mev for bismuth, and about 70 to 80 Mev for gold, for both protons and deuterons. For alpha particles the fission cross sections of bismuth and gold are constant as a function of the alpha-particle energy. This fact would seem to indicate that if the "threshold energy" for fission with alpha particles is the same as for protons and deuterons, then the probability that an alpha particle transfers at least this threshold energy for fission is independent of the initial energy of the alpha particle (in the energy region 200 to 400 Mev).

B. Comparison to Total Inelastic Cross Sections

The fission cross sections obtained in this experiment were compared to the total inelastic cross sections as measured by attenuation experiments.[46] The results of this comparison are summarized in Table VII, and plotted in Figs. 22 and 23.

Several conclusions can be drawn from the data in Table VII;

(a) For U^{238} and U^{235} fission is the most probable inelastic process for all types of incident particles at all energies investigated in this experiment.

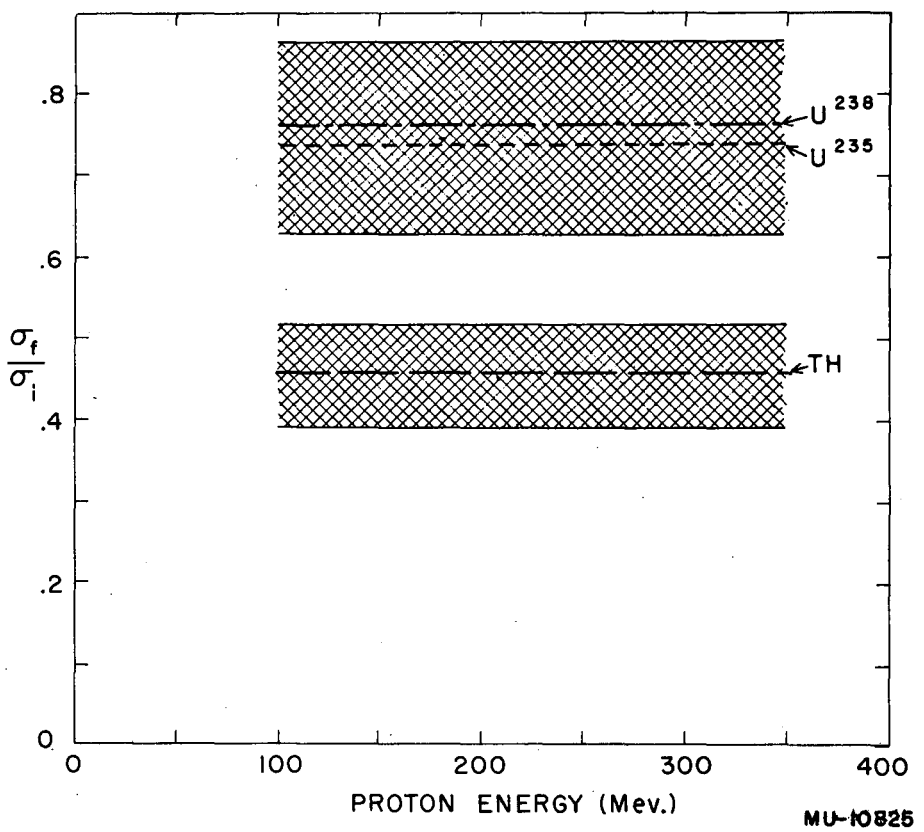

Fig. 22. Ratio of the fission cross section, σ_f, of U^{238}, U^{235}, and Th^{232} to the total inelastic cross section σ_i of natural uranium for protons. The total inelastic cross sections were obtained from the data of Millburn, Birnbaum, Crandall, and Schecter.[46]

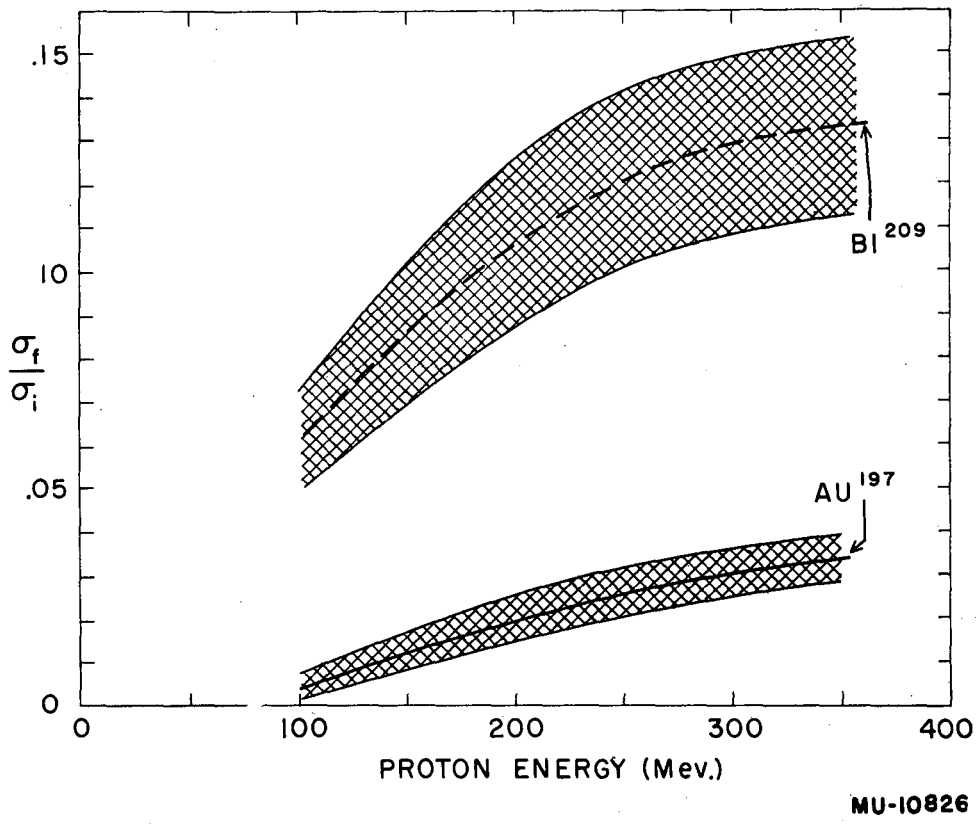

Fig. 23. Ratio of the fission cross sections, σ_f, of Bi^{209} and Au^{197} to the total inelastic cross section of lead, σ_i, for protons. The total inelastic cross sections were obtained from the data of Millburn, Birnbaum, Crandall, and Schecter.[46]

Table VII

Comparison of fission and inelastic cross sections of U, Th, Bi, and Au.

Bombarding Particles	Energy (Mev)	Sample	σ_i x 10^{24}	σ_f x10^{24}	σ_f/σ_i	Remarks
Protons	305	U	1.60	1.35	0.85	
	290		1.85	1.35	0.73	
	240		1.77	1.35	0.76	
	185		1.90	1.35	0.71	
	305	Th	1.60	0.80	0.50	σ_i was not measured for Th. We have here used σ_i for U, instead.
	290		1.85	0.80	0.43	
	240		1.77	0.80	0.45	
	185		1.90	0.86	0.42	
	305	Bi	1.48	0.19	0.13	σ_i was not measured for Bi. We here have used σ_i for Pb instead.
	290		-	0.20	-	
	240		1.57	0.16	0.10	
	185		1.55	0.15	0.10	
	305	Au	1.48	0.04	0.03	σ_i was not measured for Au. We have here used σ_i for Pbinstead.
	290		-	0.05	-	
	240		1.57	0.04	0.03	
	185		1.55	0.03	0.02	
Deuterons	160	U	3.81	2.0	0.53	σ_i is inelastic cross section of U.
	160	Th	3.81	1.3	0.34	
	160	Bi	3.55	0.23	0.06	σ_i is inelastic cross section of Pb.
	160	Au	3.44	0.04	0.01	
Alpha particles	240	U	4.33	2.3	0.53	σ_i was calculated from the data in Reference 46.
	240	Th	4.33	1.7	0.40	
	240	Bi	3.95	0.65	0.16	
	240	Au	3.95	0.22	0.06	

The inelastic cross sections were obtained from the data of Millburn, Birnbaum , Crandall, and Schecter.[46]

(b) The ratio σ_f/σ_i for U^{238}, U^{235}, and Th^{232} seems to be roughly independent of the type of bombarding particle used. In other words, the fission probability for these elements is independent of how the target nucleus is excited.

(c) The reason for the rather low ratio, σ_f/σ_i, for deuterons on bismuth and gold can best be understood if we remember that a deuteron, because of its loose binding, can make an inelastic collision without transferring much energy to the struck nucleus. Since the fission of bismuth and gold requires at least 50 Mev, it is not unreasonable that σ_f/σ_i is lower for deuterons than for protons or alpha particles.

(d) For 340-Mev protons on U^{238} the difference between the total inelastic cross section of about $1.75 \times 10^{-24} cm^2$ and the fission cross section of $1.35 \times 15^{-24} cm^2$ is about $0.4 \times 10^{-24} cm^2$. This value is in agreement with a chemical determination of the spallation cross section of U^{238} bombarded by 340-Mev protons.[47]

C. Dependence of the Fission Cross Section on the Atomic Number of the Target Nucleus

The results of this experiment indicate that the relative fission probabilities, as well as the fission cross sections, decrease strongly with decreasing atomic number for all types of bombarding particles. Furthermore, the high-energy fission cross sections of uranium seem to be independent of whether U^{235} or U^{238} is used.

D. Excitation Energy of the Struck Nucleus

The data of Table II indicate that on the average approximately one-third of the bombarding particle's initial momentum is transferred to the fissioning nucleus for 190- and 340-Mev protons, and for 240- and 375-Mev alpha particles. If we use the rather crude assumptions about the collision process that were set forth in Section III B-8, we find that for protons this amount of momentum transfer corresponds to an excitation energy in the struck nucleus of about 100 to 150 Mev

(see Table III). Monte Carlo calculations by McManus and Sharp[48] for 400-Mev protons on uranium yield a value of 94 ± 10 Mev for the most probable amount of excitation energy in the struck nucleus after the emission of the cascade particles. It must be pointed out that our estimates of the excitation energy are extremely crude and should therefore be used only to show that our results are reasonable in the light of the theoretical predictions.

E. Comparison to Other Experiments

In Figs. 7-21 we have summarized all of the heretofore published high-energy charged-particle-induced fission cross sections for U^{238}, U^{235}, Th^{232}, Bi^{209} and Au^{197}. It is readily apparent that these cross sections seem to depend not only on the type of incident particle and its energy, but to some extent also on the method of measurement. The high-energy fission cross sections obtained by Jungerman,[10] which are considerably lower in all cases than the results of the work reported here, are not included in the graphs because they are believed to be in error. A possible reason for assuming Jungerman's work to be incorrect is that it was done with electrically deflected beams, which had pulses of about 0.1-μsec duration. These small-duty-cycle beams created much larger amounts of ionization in the fission chamber during the resolving time of the fission detector than in this experiment. These large bursts of ionization may have caused the ion chamber used in Jungerman's experiment to operate unreliably.

F. Applications

A fission detector loaded with plates of uranium or thorium could be used to monitor beams of high-energy charged particles and neutrons. Such a monitor would have the advantage of being almost independent of the energy of the bombarding particles over a wide range of energies (a few Mev to several hundred Mev at least). For example, in order to get 1 monitor count per 10^4 neutrons we would require an effective sample thickness of about 30 mg/cm^2 for uranium (assuming the neutron-induced fission cross section of uranium to be the same as the proton-induced fission cross section at high energies).

CHARGED PARTICLE EXPERIMENTS ON URANIUM-233, URANIUM-234, URANIUM-236, AND NEPTUNIUM-237

I. INTRODUCTION

Although no significant difference was observed between the fission cross section of U^{238} and U^{235}, it was considered of interest to determine if there is any difference between the fission cross sections of other uranium isotopes bombarded by high-energy charged particles. The experiment performed consisted of measuring the total fission cross sections of U^{233}, U^{234}, U^{236}, and Np^{237} when bombarded by (a) 195-, 244-, 290-, and 336-Mev protons; (b) 118- and 191-Mev deuterons, and (c) 240-, 307-, and 375-Mev alpha particles. Unfortunately, severe time limitations were imposed on the experiment, so that the results could not be obtained to the same degree of accuracy as the results of the preceding work. The same cancellation-type ionization chamber as was used earlier was used in this experiment.

II. APPARATUS

A. Samples

All the samples used in this phase of the experiment were prepared by electrodeposition. The technique is described in Appendix I. The samples were deposited onto 2-by-2-inch pieces of nickel foil, 0.00035 inch thick. The area of the deposits was circular and approximately 1-3/4 inches in diameter. The average thickness of each sample was determined by alpha counting the entire sample in a calibrated low-geometry alpha scintillation counter, and dividing the total activity of the sample by (1) the area of the deposit ($\sim$13.45 cm^2), and (2) the specific activity of the sample. From a knowledge of the isotopic purity of each sample (all samples were $\geq$89% pure) the thickness of the deposits could be calculated. These thicknesses ranged from 0.25 to 0.75 mg/cm^2. Unfortunately, the uniformity of the samples varied by as much as 30% over the area of a sample. This large fluctuation in sample thickness was washed out to some extent by the fact that the beam intensity was quite uniformly spread over the area

of the 1-inch-diameter collimator used in these bombardments. This was especially true at the lower beam energies, where the internal absorber acted as a diffusing screen so that the beam intensity was very uniform over the cross-sectional area of the beam. The uniformity was later verified by examining photographs of the profile of the beam.

Because of the relatively low specific activity of the U^{236} sample a small amount of contamination could seriously affect the thickness as determined by alpha counting. We therefore decided to determine the thickness in this case by making a colorimetric and a gravimetric analysis of the amount of uranium on the plate. The results of these analyses agreed with each other but differed by about 40% from the results obtained by alpha counting. This would indicate that this sample was at least slightly contaminated with a substance of higher activity. Spectroscopic tests indicated no radioactive substances except uranium were present in detectable amounts. Hence, the sample was probably slightly contaminated with another isotope of uranium.

III. PROCEDURE

The procedure used in these runs closely parallels that used in the earlier runs with the "common" isotopes. However, because of the relatively high alpha activity of some of the samples, such as U^{234} and U^{233}, several slight modifications had to be made in the equipment in order to minimize the effect of the large pulses observed when several alpha particles produced ionization during the five-microsecond resolving time of the electronic equipment. There were essentially two ways by which this problem of alpha pile-up could be attacked: (1) By making the resolving time of the apparatus shorter; and (2) by counting only during the time that the beam actually passes through the chamber, or in other words matching the duty cycle of the electronic equipment to the duty cycle of the cyclotron. Therefore, during the actual runs we changed the clipping time of the linear pulse amplifier from five microseconds to one microsecond, and we again used an electronic gate which allowed the scalers to count only while the beam was actually passing through the fission chamber. Whereas in previous runs the only type of background was caused by the effects of beam ionization in the chamber, in these runs the effects of alpha pile-up were also important, especially with the lowest-biased scalers; therefore, extrapolations of the integral bias curves to zero bias were usually made without considering those points on the bias curve where the background effect was equal to or greater than the true fission rate. In analyzing the data we subtracted (1) the pulses caused by the beam in passing through the chamber or the sample backing (normalized to the number of charged particles through the bombarded sample), (2) the number of alpha pile-up pulses observed at each bias setting of the scalers (normalized to the duration of time needed for observing the fission counts). In order to insure that all of the equipment was functioning properly, the U^{235} sample used earlier was again exposed to the beam along with these new samples. In all cases the U^{235} results agreed to within the statistics (about ± 3%) with the earlier work.

IV. RESULTS

The results of these experiments are summarized in Table VIII. Only standard deviations due to counting statistics are indicated in this table. In addition to the statistical errors the following systematic errors may be ascribed to this part of the experiment: (a) determination of sample thickness, ± 3%; (b) uniformity of sample thickness over the area of the sample, ± 15%; (c) self-absorption of fission fragments in the sample material, ± 5%; (d) isotopic purity of the samples, ± 4%; (e) extrapolation to zero bias, ± 8%; (f) momentum transfer to the struck nucleus, ± 1.5%, (g) determination of beam energy, ± 1%; (h) calibration of beam monitor, ± 3%; (i) geometry of chamber, ± 0.5%. When these errors are compounded, a total systematic error of 19% may be ascribed to this experiment. The accuracy of the total cross sections may again be obtained by combining the above systematic errors with errors due to counting statistics indicated in Table VIII.

V. DISCUSSION

The results of this part of the experiment indicate that there is no appreciable difference between the fission cross sections of U^{233}, U^{234}, U^{235}, U^{236}, Np^{237}, and U^{238} for all types of bombarding particles at all energies investigated. Therefore, the conclusions arrived at in the preceding section with respect to the fission cross sections of uranium apply not only to U^{238} and U^{235} but also to all the isotopes investigated in this part of the experiment.

Table VIII

Charged-particle-induced fission cross sections for U^{233}, U^{234}, U^{236} and Np^{237}
(In Units of 10^{-24} cm^2)

Bombarding Particle	Energy (Mev)	U^{233}	U^{234}	U^{236}	Np^{237}
Protons	336	1.27 ± .02	1.45 ± .02	1.40 ± .02	1.27 ± .02
	292	1.18 ± .03	1.27 ± .03	1.26 ± .02	1.30 ± .03
	244	1.22 ± .03	1.45 ± .03	1.33 ± .02	1.22 ± .03
	193	1.20 ± .03	1.31 ± .03	1.36 ± .02	1.20 ± .03
Deuterons	192	1.97 ± .04	2.14 ± .05	2.14 ± .04	1.87 ± .04
	119	2.01 ± .06	2.14 ± .06	2.29 ± .04	2.06 ± .05
Alpha Particles	379	2.46 ± .04	2.62 ± .05	2.65 ± .05	2.24 ± .05
	372	2.37 ± .04	2.45 ± .05	2.43 ± .06	2.25 ± .04
	309	2.22 ± .06	2.32 ± .04	2.51 ± .06	2.07 ± .08
	309	2.27 ± .06	2.24 ± .05	2.31 ± .06	2.28 ± .06
	243	2.43 ± .07	2.60 ± .06	2.54 ± .07	2.03 ± .08
	242	1.98 ± .09	2.25 ± .09	2.14 ± .14	1.98 ± .14

PHOTOFISSION EXPERIMENTS

I. INTRODUCTION

Several experiments have been performed to investigate photofission cross sections in the energy region 100 to 300 Mev.[49-53] In the experiment reported herein we have investigated the photofission cross sections of U^{238}, U^{235}, Th^{232}, Bi^{209}, and Au^{197} for photons produced in bremsstrahlung spectra whose maximum energies ranged from 100 to 500 Mev. The energy region 100 to 335 Mev was investigated for the most part at the University of California synchrotron, whereas the higher-energy data were obtained at the synchrotron of the California Institute of Technology. The cancellation-type ionization chamber used for the charged-particle experiments was also used for these photofission experiments.

II. APPARATUS AND METHOD

A. Fission Chamber

The ionization chamber used in this experiment is described in the preceding section. The beam was again passed through the chamber in the direction CBA. This orientation was chosen in order to minimize the effect of the electron-positron pairs produced in the sample backing. The distance from the thin entrance window to the sensitive region of the ionization chamber was ~4 inches, so that any pairs produced in the entrance window had a relatively small chance of producing uncancelled pulses in the sensitive region of the ionization chamber. In order to minimize pair production in the gas, the chamber was filled with 1 atmosphere of hydrogen. Finally, pair production in the electrodes was kept small by making them out of 140 $\mu g/cm^2$ aluminum foil.

Chronologically, the photofission runs were mostly made before the charged-particle experiments were carried out. In these early runs only one scaler was used. It was only in the last photofission run at the Berkeley synchrotron that we switched to the system of using six scalers

simultaneously in order to obtain an integral bias curve at each point. Otherwise the electronic arrangement was identical to that described earlier (see page 8).

B. Samples

The samples used in these photofission runs were identical to those used for the charged-particle experiments with the exception of Th^{232} and Au^{197}. These samples had thicknesses of 0.88 g/cm^2 and 1.07 g/cm^2 respectively. The Th^{232} sample was prepared by painting as described previously, whereas thin foil was used for the gold sample. The loss of fissions due to self-absorption in the samples was determined with charged particles (see Table I), and the same corrections were applied to this work.

C. Method

Figure 24 shows a diagram of the experimental arrangement at Berkeley. The bremsstrahlung beam was generated in a 0.020-inch platinum target, collimated to 3/4-inch diameter, passed through a sweep magnet, then through the fission chamber, and finally into a replica of a thick-walled ionization chamber, the original of which was calibrated by Dr. R. Wilson at Cornell. At the calibration point, 315 Mev, 3.73×10^{18} Mev passes through the chamber per coulomb collected.[54] The group at California Institute of Technology ("Cal Tech") calibrated a similar "Cornell" chamber at 500 Mev. They find a value of 4.13×10^{18} Mev/coulomb.[55] A linear energy dependence of 5.3% per 100 Mev was therefore assumed, and this correction has been applied to obtain the number of equivalent quanta at various energies.

In order to determine the maximum energy of the synchrotron beam a pair spectrometer designed by Dr. Robert W. Kenney was used at Berkeley with the Cornell chamber removed. The electron-pair trajectories in vacuum, coupled with a nuclear resonance determination of the pair-spectrometer magnetic field, determine the energy of the bremsstrahlung beam on an absolute scale. The operation of this

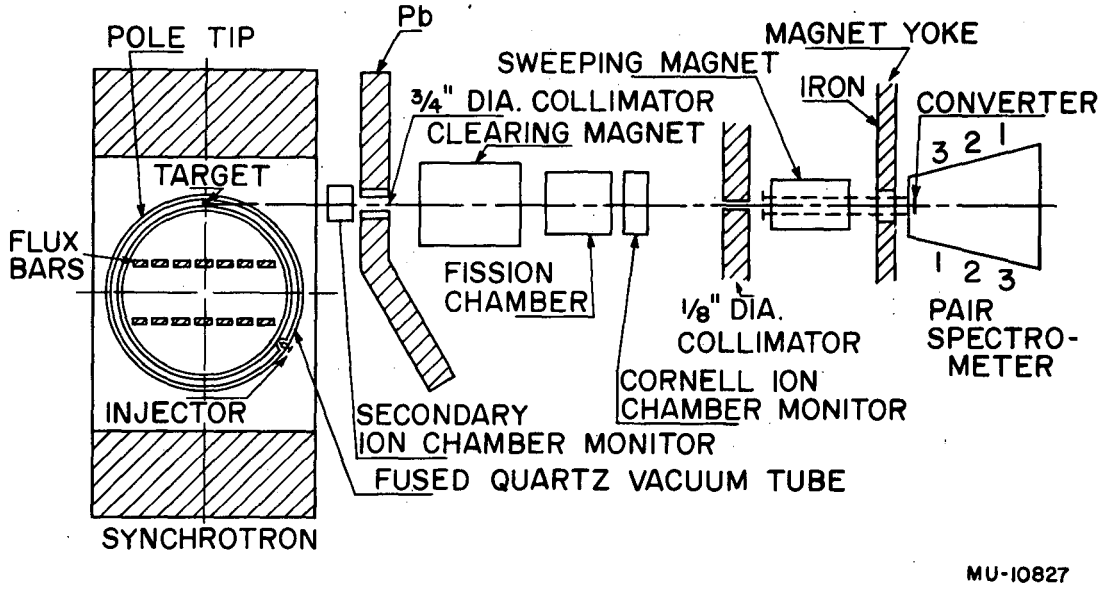

Fig. 24. Schematic diagram of the experimental arrangement at the Berkeley synchrotron. (The drawing is not to scale.)

spectrometer is described in more detail by McDonald.[56] The maximum energy of the beam was determined in this way for each energy studied.

The synchrotron at Berkeley has a repetition rate of 6 cycles/sec and the beam comes out in a 2500-μsec time interval when operating at full energy (337 Mev). However, when the beam energy was reduced appreciably below its maximum value the beam spilled out in a time of the order of 10 μsec. This "spiked" beam made it necessary to run at rather low beam intensities because of the chance of losing fission counts by having several arrive during the resolving time of our apparatus (5 μsec). This circumstance also made the energy determination more difficult because low beam intensities were necessary to reduce accidental counts in the pair spectrometer to a reasonable level. In the last run at Berkeley (run No. 4) it became possible to extend the duration of the beam to one msec at reduced energies.

The experiment at Cal Tech was carried out with the same fission chamber and electronic apparatus as was used at Berkeley. The path from the 0.016-inch copper bremsstrahlung target to the fission chamber was somewhat longer so that the solid angle was reduced compared to the Berkeley setup. The beam there was 1 msec in duration at all energies, and had a repetition rate of 1 pulse per second. The increased duty cycle at reduced energies greatly facilitated gathering reliable data. The maximum beam energy was determined to 1% by use of the calibrated rf pulse timing equipment of the Cal Tech synchrotron.[57]

III. PROCEDURE

A. Slow Neutrons

Before each photofission run a Po-Be source encased in paraffin was placed adjacent to the fission chamber with the U^{235} sample in place. By observing the resulting fission pulses we were able to check the over-all operation of the apparatus. In particular, we were able to determine if impurities in the hydrogen gas affected the electron-collection efficiency by observing an integral bias curve.

B. Alignment

The alignment of the fission chamber was checked with photographic film. These pictures were taken every time the chamber was moved or the operation of the machine changed markedly.

C. Cancellation

At the start of a photofission run we first minimized the counting rates with the blank sample in position. This was done by adjusting the voltage on the cancellation electrode C unitl a minimum signal was observed in an oscilloscope. Since this signal was strongly dependent on the beam intensity and its distribution in time, the maximum useful beam strength was limited in some cases (low-cross-section samples in a "spiked" beam.)

The background due to noncancellation of the beam ionization, as determined with the aluminum blank target, was less than 2% for U^{235}, U^{238}, and Th^{232} at all energies. For bismuth this background was less than 10% and for gold it was less than 23% at all energies. This background was quite constant for a given beam intensity at a given energy, and thus could be subtracted with good reliability.

D. Pile-Up of Fission Pulses

In most cases the limiting beam strength was determined by the resolving time of the electronic equipment (5 μsec). In order to keep the loss of fissions due to pile-up of fission pulses to less than 1%, a counting rate of less than 36 counts/min had to be used with the "spiked" beam. This counting rate was determined experimentally by measuring the counting rate per microcoulomb collected in the Cornell chamber versus the reciprocal of the beam intensity. This curve is shown in Fig. 25.

E. Variation of High Voltage on Electrodes B and C

The counting rate per microcoulomb collected was also measured versus the voltage on the collecting and cancellation electrodes, and a suitable plateau was obtained. The curves look very much like those of Fig. 4. The final operating voltages were B = 1500 v, C = 3300 v for most of the runs.

F. Integral Bias Curve

A similar plateau was also taken of counting rate per microcoulomb versus the pulse height necessary to trip our scaler. This curve was used to extrapolate the observed counts to zero bias, and is similar to the bias curve shown in Fig. 4. In run No. 4 at Berkeley six scalers were used at 2.5-volt bias intervals, giving a five-channel integral pulse spectrum. In this manner a bias plateau was obtained for each sample at each energy. We believe the data collected in this manner to be more reliable because of the increase in information available.

G. Gating of Scalers

In all runs at Berkeley an electronic gate was used that allowed our scalers to count only while the beam was on. Electrical disturbances from the synchrotron operation were quite prominent if the gate was not used.

H. Neutrons

The effect of neutrons was estimated by use of the U^{235} sample which should be the most neutron-sensitive. There are two main sources of neutrons, (1) neutron contamination of the beam (probably due to photoneutrons produced in the walls of the doughnut and the collimator), (2) photoneutrons produced in the aluminum sample backing. The effect of the neutrons in the beam was checked by shifting the fission chamber six inches to one side so that it just cleared the beam. The resulting counting rate was less than 2% of the rate with the same intensity photon beam passing through the chamber. The effect of the photoneutrons produced in the sample backing was investigated by the placing a sheet of aluminum, 7/8 inch thick, immediately following the fission chamber. Although this amount of aluminum was sufficient to increase the effective aluminum backing from 0.001 inch to 0.026 inch (assuming isotropic photoneutron emission), no effect was observed on the fission cross section of U^{235}.

I. Electron Contamination

A check was made of the effect of electron contamination of the beam on the fission cross section by inserting a sweep magnet immediately in front of the fission chamber. No effect was observed.

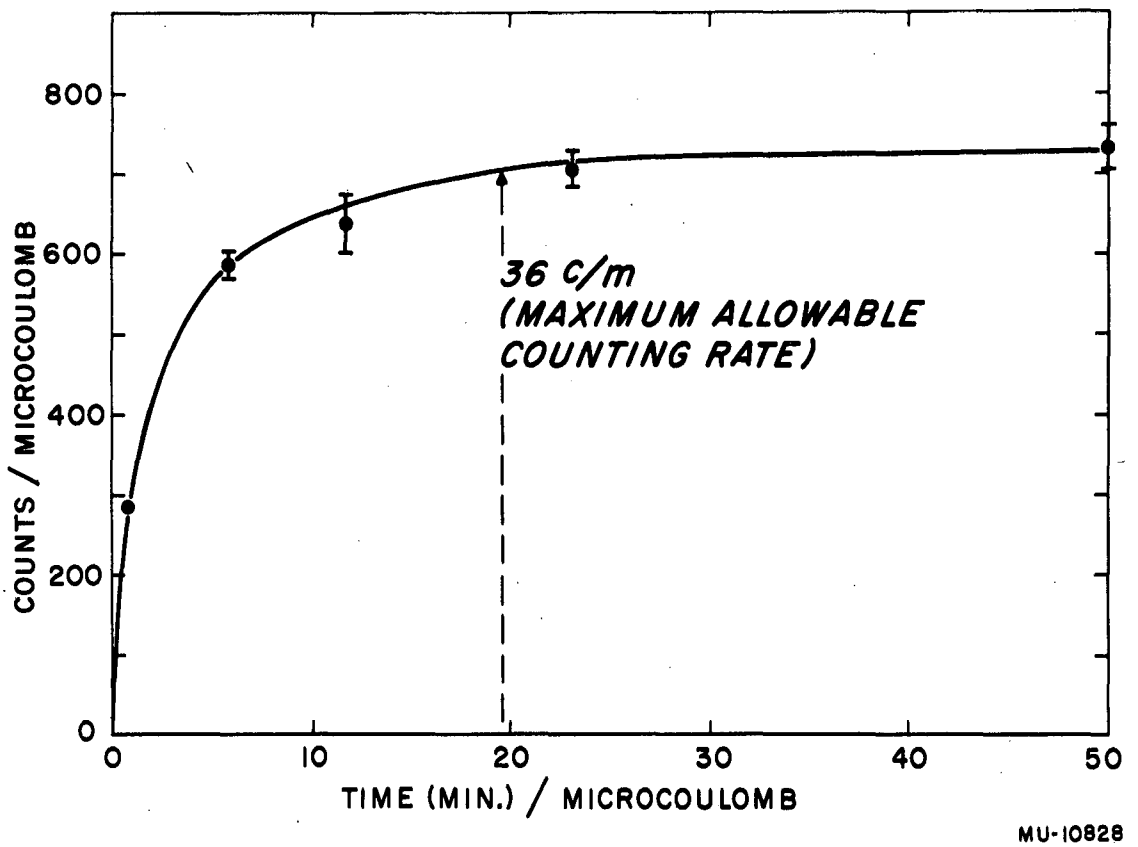

Fig. 25. Counting rate plotted against the reciprocal of the beam intensity for a "spiked" beam at the Berkeley synchrotron. The ordinate shows the number of counts observed while the beam monitor collected 1 microcoulomb of charge. The abscissa shows the time (in minutes) necessary to charge the beam monitor to 1 microcoulomb.

IV. EXPERIMENTAL RESULTS

The fission cross section per equivalent quantum σ_Q, for both the Berkeley and Cal Tech experiments, is presented in Table IX and plotted in Figs. 26 and 27. The energy scale is logarithmic, since in this presentation the slope of the curve represents the fission cross section if a rectangular bremsstrahlung spectrum is assumed. (See Appendix II.) It will be noted that the change in accelerators shifts the cross section per equivalent quantum by about 15% for U^{235}, U^{238}, and Th^{232} at the joining energy of 335 Mev. For bismuth, shown in Fig. 27, the change of accelerators is perhaps masked by the steepness of the σ_Q curve. Since the cross section per equivalent quantum depends not only on the calibrated ionization chamber and its associated electronic equipment, but also on the value ascribed to the maximum beam energy, errors in any of these variables on either accelerator could lead to the discrepancy in the absolute value for σ_Q at 335 Mev. In all cases, however, the slopes of the σ_Q curves seem to be continuous.

The data obtained for U^{238}, U^{235}, and Th^{232} can most easily be fit with a straight line having a slope corresponding to a cross section of 25 to 50 x 10^{-27} cm^2 in the energy region 200 to 500 Mev.

An analysis of the bismuth fission cross section, using Schiff bremsstrahlung spectra[58] and taking into account the dependence of the spectrum shape on the maximum energy of the bremsstrahlung, was made by the method described by Katz and Cameron.[59] We found, for a given smoothed plot of the σ_Q curve, that the cross section increased about 15% but had about the same shape as given by the rectangular bremsstrahlung spectrum. It was also noted that the arbitrariness allowed in drawing a smooth curve through the experimental points creates the same order of uncertainty as the difference between the two methods of spectrum analysis. We have therefore used the rectangular spectrum because of its simplicity. The fission cross sections resulting from this analysis are shown in Fig. 28. They are derived from the smoothed curve shown in Fig. 27.

Table IX

Fission cross section per equivalent quantum for 100- to 500-Mev photons
(In Units of 10^{-27} cm^2)

Maximum energy of bremsstrahlung spectrum (Mev)	U^{238}	U^{235}	Th^{232}	Bi^{209}	Au^{197}
502	...	...	...	7.08 ± .20	...
501	...	...	65.8 ± 2.0	...	...
500	...	247 ± 10	...	6.56 ± .20	...
498	...	...	...	...	1.57 ± .09
480	159 ± 5	...	62.4 ± 2.0	...	...
480	...	...	67.0 ± 2.1	...	...
479	...	...	...	6.17 ± .20	...
476	...	254 ± 6	67.0 ± 2.2	6.16 ± .20	...
476	...	261 ± 7	61.2 ± 2.0	...	...
471	...	...	63.4 ± 1.3	...	...
466	...	...	...	6.25 ± .20	...
452	...	...	...	6.10 ± .18	...
450	...	...	...	...	1.42 ± .14
434	...	...	61.5 ± 2.0	...	...
430	157 ± 4	...	54.9 ± 2.0	5.48 ± 0.17	...
430	148 ± 4	252 ± 7	57.0 ± 1.8	...	...
408	...	...	...	5.09 ± .17	...
400	...	...	...	...	1.23 ± .11
389	...	...	60.5 ± 2.0	...	...
385	150 ± 3	...	50.5 ± 1.5	4.71 ± .14	...
385	153 ± 4	...	51.5 ± 1.5	...	...
364	...	...	...	4.06 ± .12	...
361	...	...	...	3.95 ± .12	...
350	...	...	...	...	0.86 ± .10
337	183 ± 9	274 ± 8	59.5 ± 1.3	3.19 ± .09	...
335	168 ± 7	260 ± 6	60.8 ± 3.1	3.27 ± .33	...
335	144 ± 4	235 ± 6	51.3 ± 1.5	3.12 ± .13	...
335	147 ± 3	...	49.8 ± 1.5	...	...
334	181 ± 1	274 ± 1	58.5 ± 0.5	2.82 ± .07	...
302	163 ± 5	244 ± 6	53.0 ± 1.1	...	...
301	...	...	...	...	0.72 ± .08
300	163 ± 5	...	...	...	...
291	168 ± 5	276 ± 5	61.2 ± 1.8	...	...
285	173 ± 5	...	...	2.26 ± .18	0.78 ± .06
285	...	...	55.7 ± 1.3	1.85 ± .13	...
277	167 ± 2	248 ± 2	54.5 ± 1.3	2.10 ± .18	0.19 ± .03
257	...	...	46.8 ± 1.1	1.76 ± .09	0.486± .034
250	...	...	...	1.78 ± .22	0.33 ± .07
249	151 ± 3	239 ± 6	50.2 ± 1.4	...	...
244	170 ± 5	270 ± 7	51.3 ± 1.3	...	...
232	...	239 ± 4	...	...	...
210	...	...	...	1.18 ± .28	...
207	154 ± 4	244 ± 8	42.8 ± 1.2	...	...
200	...	...	...	1.30 ± .24	0.31 ± .09
183	165 ± 5	260 ± 7	47.1 ± 1.3	...	...
180	138 ± 4	219 ± 6	42.3 ± 1.3	...	...
179	160 ± 3	247 ± 10	43.3 ± 1.1	0.68 ± .09	...
150	...	...	...	0.61 ± .12	...
143	147 ± 4	226 ± 6	43.3 ± 1.4	...	...

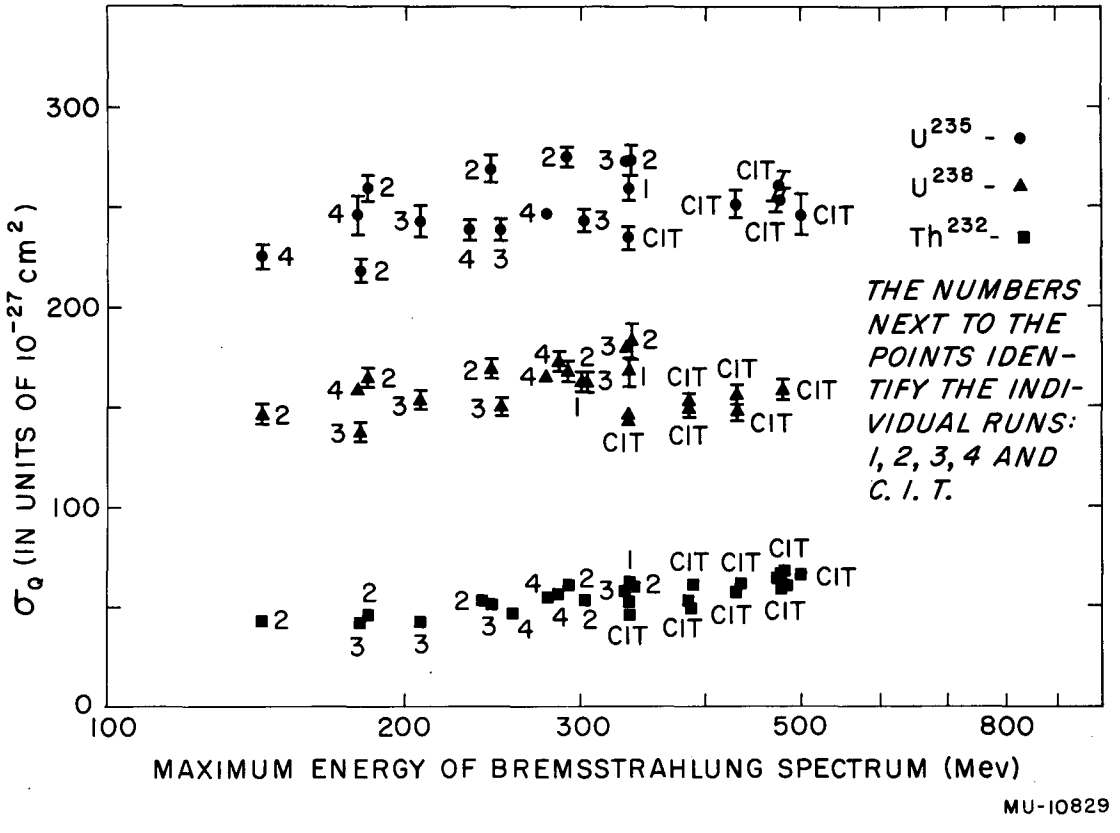

Fig. 26. Photofission cross section per equivalent quantum σ_Q versus bremsstralung energy for U^{235}, U^{238}, and the Th^{232}. The errors indicated on the points are standard deviations due to counting statistics only.

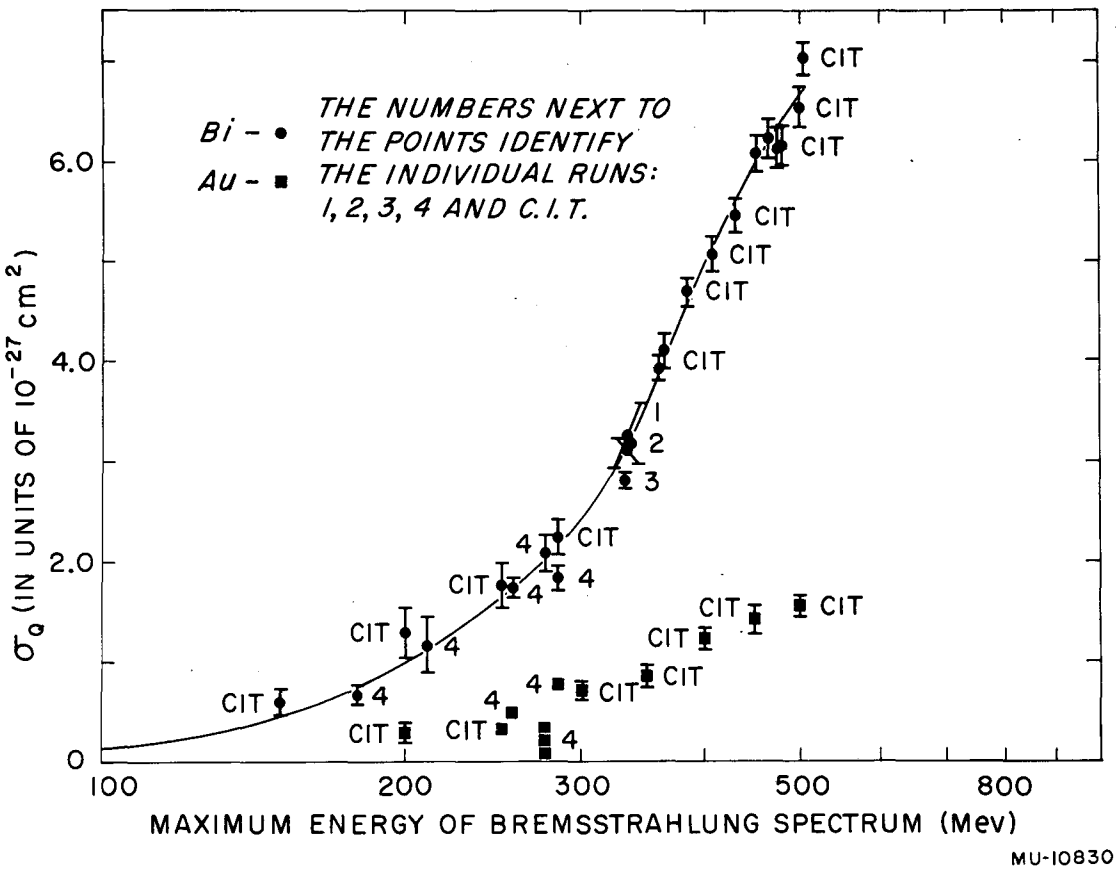

Fig. 27. Photofission cross section per equivalent quantum, σ_Q, versus bremsstrahlung energy for Bi^{209} and Au^{197}. The errors indicated on the points are standard deviations due to counting statistics only.

It should be noted that the use of a longer beam duration in the fourth run at Berkeley gives essentially the same cross sections for U^{235}, U^{238}, and Th^{232} as obtained in the earlier runs. It also allowed a more reliable measurement of the bismuth cross section at reduced energies. On previous runs with bismuth at reduced energies the uncancelled beam-ionization background made measurements untrustworthy. However, even in the fourth run there was still a residual background, which is apparently electrical in nature, that made the measurements with the gold target at Berkeley unreliable. It should be mentioned also that the 200-Mev point obtained for gold at Cal Tech is based on 11 counts and the 300-Mev point on 83 counts, so that the cross sections reported are quite provisional. This scarcity of counts arises from the fact that both the fission cross section and the beam strength decrease markedly as the energy is decreased, so that the time necessary to increase the number of counts becomes prohibitive. In addition to the statistical errors indicated on the graphs the σ_Q curves can have systematic errors due to errors in sample thickness, ± 7%; errors in calibration for the number of equivalent quanta including its energy dependence, ± 8%; error in extrapolation to zero bias, ± 5%; errors in determination of the beam energy, ± 2%. A total probable systematic error of ± 13% can thus be ascribed to the experiment.

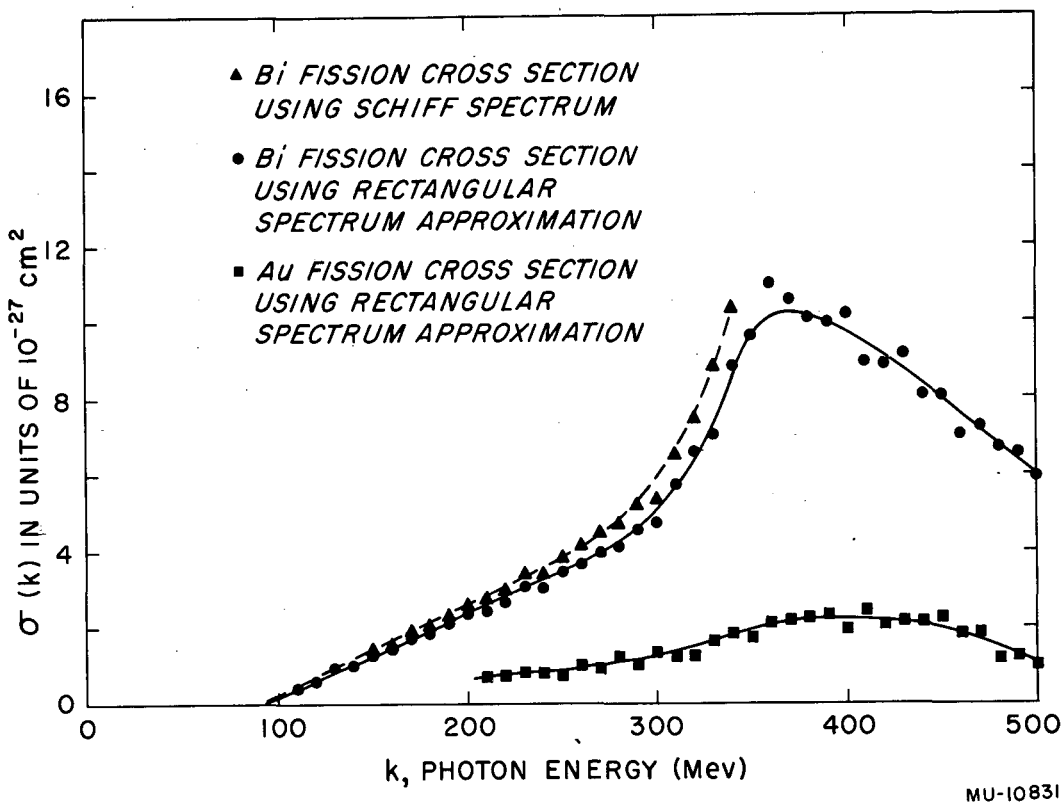

Fig. 28. Photofission cross sections σ (k) of Bi and Au as a function of photon energy. These curves were obtained from a smoothed plot of the data in Fig. 27. The dotted curve was calculated by assuming a Schiff bremsstrahlung spectrum that varied with energy, using the method of Katz and Cameron.[59] The solid curves were calculated in the rectangular spectrum approximation.

V. DISCUSSION

A. Bismuth and Gold

From the data in Fig. 27 we note that the photofission cross sections per equivalent quantum for bismuth and gold both increase rapidly as the maximum energy of the bremsstrahlung spectra is increased, especially in the energy region near 300 Mev. When the σ_Q curve is analyzed, we find that the photofission cross section of bismuth, σ (k), increases with increasing photon energy k until it reaches a maximum value of about 10×10^{-27} cm^2 at about 400 Mev. With the present fit of the σ_Q data, the σ (k) curve shows a resonance type of behavior near 450 Mev; i.e., the cross section seems to decrease again above 450 Mev. The cross sections for gold show a similar behavior, reaching a maximum value of about 2×10^{-27} cm^2 at 400 Mev. It must be emphasized, however, that the arbitrariness involved in drawing a smooth curve through the experimental points is such that σ (k) may not be decreasing above 450 Mev. In order to definitely determine whether or not this resonace type of behavior of the photofission cross section is real, experiments should be carried out at higher energies (500 to 1000 Mev).

Because of the similarity of the curves of σ (k) versus k for photofission and for the photoproduction of mesons from nucleons, it is tempting to relate the two processes. A possible interpretation of our results, first suggested by Bernardini, Reitz and Segrè,[50] is that internally produced mesons are reabsorbed within the nucleus in which they are created, thus giving an additional mechanism by which a nucleus may absorb the photon energy. Let us pursue this possibility a little further. From the photofission data we find that the photofission cross sections of bismuth and gold reach their maximum value at about k = 400 Mev. However, the data of Oakley and Walker,[60] Walker, Oakley and Tollestrup,[61] Walker, Peterson, Teasdale, and Vette,[62] and Tollestrup, Keck and Worlock,[63] indicate that the peak of the photomeson production from hydrogen occurs near 300 Mev. Furthermore, the width of the photofission "resonance" (if we assume that it is real) is somewhat broader than the corresponding width in

the case of photomeson production from hydrogen. These discrepancies can be resolved if we recall that there are several factors influencing photofission that are not present in the photoproduction from hydrogen. First, the motion of the nucleons inside the nucleus causes a broadening of the nucleon-photomeson resonance because of the Doppler effect. Those nucleons moving toward the impinging photon see higher-frequency photons than those at rest. Conversely, those nucleons moving away from the beam see lower-frequency photons. Second, the effect of the Pauli principle is such that when a photomeson is produced from a nucleon in the nucleus, the struck nucleon must go into an unoccupied nucleon state. Since the low-energy nucleon states are already filled, the production of high-energy mesons is favored. This effect therefore causes the resonance to shift toward higher energies. Third, the close proximity of the nucleons inside the nucleus may cause interference effects in the production of mesons. It is not clear, however, what effects, if any, this factor may have either in broadening or in shifting the resonance curve. Last of all, the reabsorption of the meson within the nucleus in which it was created depends on the energy of the meson. Various experimenters have found[64-71] that the absorption mean free path of mesons in nuclear matter decreases with increasing meson energy. Therefore, the absorption of high-energy mesons is favored, which again tends to shift the resonance toward higher energies. Thus, the experimental data on the photofission of bismuth and gold are consistent with the interpretation of reabsorption of internally produced photomesons.

We can use the results of the charged-particle experiments to make a rough estimate of the total photonuclear cross sections of bismuth and gold. From the data in Table VII, we see that the fission probabilities for bismuth and gold at high energies are about 0.15 and 0.04 respectively. If we assume the same fission probabilities to hold in the case of photofission, we obtain a total photonuclear cross sections of about 70×10^{-27} cm^2 for bismuth and about 60×10^{-27} cm^2 for gold at 400 Mev. It is interesting to note that if we assume that at 300 Mev the average cross section for both charged[62,63] and

neutral[60,61,72] photomeson production from nucleons is 2×10^{-28} cm^2 then $\sigma_T \backsim A\,(\bar{\sigma}_c + \bar{\sigma}_0) \backsim 200 \times 4 \times 10^{-28} = 80 \times 10^{-27}$ cm^2, which is in good agreement with the values obtained above.

The similarity of the σ_Q curve for bismuth to the photostar excitation function per equivalent quantum obtained by Peterson[73] is also interesting, and suggests that the same mechanism might account for both phenomena.

URANIUM-238, URANIUM-235, AND THORIUM-252

Since the photofission thresholds for U^{238}, U^{235}, and Th^{232} are all about 5 Mev,[74] it is reasonable to expect that a large contribution to the photofission cross section per equivalent quantum for these elements occurs at low energies, i.e., in the "giant resonance" region.[75] Any meson effects of the type observed in bismuth and gold would presumably be masked by the effects of the low-energy quanta. From Fig. 26 we see that the σ_Q curves for U^{238}, U^{235}, and Th^{232} apparently increase with increasing energy, although much more slowly than for bismuth or gold. The increase of σ_Q with increasing energy is most pronounced in Th, and smallest in U^{235}. This is to be expected, since the effect of the low-energy quanta is greatest for U^{235} and smallest for Th.

The increased photofissionability of U^{235} over U^{238} is difficult to explain. If we assume that the low-energy quanta account for most of the fission, and if neutron emission competes favorably with fission, then the following argument would predict a slightly higher fission yield for U^{235} than for U^{238}: The last neutron in U^{238} is bound more tightly than the last neutron in U^{235}, by about 1 Mev.[76] If 14-Mev quanta (the peak of the giant resonance) were to eject neutrons from both U^{238} and U^{235}, the residual U^{234} nucleus would be more excited than the residual U^{237} nucleus by about 1 Mev. If the assumption is correct that the photofission threshold is the same for U^{234} and U^{237},[74] then the U^{234} nucleus has more likelihood of being above the photofission threshold than the U^{237} nucleus. Hence, U^{235} is more likely to ultimately undergo fission than U^{238}. However, the magnitude of this effect--even

if we assume that neutron emission always precedes fission--is too small to account for the experimentally observed difference in cross sections. Another possible explanation is that U^{235} is inherently more fissionable than U^{238} by photons in the "giant resonance" region.

ACKNOWLEDGMENTS

This experiment was carried out with the help and advice of many persons. In particular I would like to thank Professor Emilio Segrè for suggesting this problem, and for his guidance and help throughout the course of the experiment. The work on photofission and much of the work on proton-induced fission was done in collaboration with Dr. John Jungerman. To him I would like to express my sincerest thanks. My thanks also go to Professor Owen Chamberlain and Dr. Clyde Wiegand for many helpful suggestions and interesting discussions. Much of the work on charged-particle-induced fission was done with the active help of Mr. Donald Keller. The assistance of Messrs. John Baldwin, David Fisher, G. A. Linenberger, and James Simmons during the various runs was greatly appreciated. Some of the samples were prepared and analyzed with the help of Messrs. Richard Sinnott, John Peck, Daniel O'Connell, and Larry Williams.

I acknowledge with pleasure the wholehearted cooperation extended to us by Professor R. F. Bacher and the staff of the California Institute of Technology synchrotron, and in particular to Dr. V. Z. Peterson, who assisted us throughout the run there.

Assistance with the pair magnet monitor at Berkeley by Dr. Robert Kenney, Dr. Charles McDonald, and Mr. John Anderson is gratefully acknowledged. Thanks are also due to Mr. William Imhoff, who supervised the construction of replicas of the Cornell ionization chambers for calibration of the Berkeley synchrotron beam. Finally, I wish to thank the staff of the Berkeley synchrotron under the direction of Mr. George McFarland, and the staff of the 184-inch synchrocyclotron under the direction of Mr. James Vale for their helpfulness throughout the course of the experiment.

APPENDIX I

URANIUM PLATING

(1) Plating Cell: The plating cell used in these electrodepositions consisted of a 1-5/8-inch diameter glass chimney mounted on a brass base plate. Watertightness was achieved with a Koroseal washer.

(2) Assembly of Plating Cell: Place the clean nickel foil (onto which the sample is to be plated) on the brass base. Place the Koroseal washer on the nickel foil and on top of the washer place the glass chimney. Attach springs or strong rubber bands between the base and the chimney. Finally put a few drops of Zapon (dilute) around the edge of the washer and allow to dry. Place the cell in a water bath that has been preheated to about 80°C.

(3) Preparation of Uranium: Boil 1 to 10 mg of uranium solution down to 2 drops. Add 2 drops of of HNO_3. Boil to complete dryness. Dissolve the uranium nitrate in 0.4M $(NH_4)_2C_2O_4$ and transfer this to the plating cell.

(4) Plating: Start the stirring motor and adjust its speed to about 60 rpm. Attach the negative lead of the power supply to a platinum wire, which should be hooked to the brass plate (and hanging out of the water bath). Turn on the power supply and adjust the voltage to 3.6 to 4.0 volts. The current should be about 100 ma/cm^2. Plate for about 30 minutes. Keep the water bath at 80°C.

(5) Cleaning of Uranium Plate: Add several milliliters of methyl alcohol to the plating cell. Turn off the stirring motor. Then remove the cell from the stirring motor and switch off the current. Draw off the methyl alcohol – oxalate solution. Repeat the methyl alcohol rinsing once or twice more. Disassemble the plating cell and rinse off the uranium plate with acetone several times. Dry the uranium plate on a hot plate.

APPENDIX II

CALCULATION OF PHOTOFISSION CROSS SECTION IN THE RECTANGULAR SPECTRUM APPROXIMATION

Let $N(k, k_0) \equiv$ number of photons in the energy interval between k and $k + dk$, for a spectrum of maximum energy k_0;

$F(k, k_0) \equiv$ energy distribution of photons in the energy interval between k and $k + dk$, for a spectrum of maximum energy k_0;

$\sigma(k) \equiv$ fission cross section for photons of energy k;

$\sigma_Q(k_0) \equiv$ fission cross section per equivalent quantum;

$Q(k_0) \equiv$ number of equivalent quanta;

$\mathcal{N} \equiv$ number of atoms per cm^2 in the sample;

$f \equiv$ observed number of fission events;

then
$$f = \sigma_Q \mathcal{N} Q = \mathcal{N} \int_0^{k_0} N(k, k_0)\, \sigma(k)\, dk \tag{1}$$

or
$$\sigma_Q = \frac{1}{Q} \int_0^{k_0} N(k, k_0)\, \sigma(k)\, dk. \tag{2}$$

The assumption of a rectangular spectrum implies that

$$F(k, k_0) = F_0 = \text{constant for } 0 \leq k \leq k_0, \tag{3}$$

$$F(k, k_0) = 0 \qquad \text{for } k \geq k_0;$$

$$Q = \frac{\int_0^{k_0} F(k, k_0)\, dk}{k_0} = \frac{F_0 k_0}{k_0} = F_0; \tag{4}$$

$$N(k, k_0) = \frac{F(k, k_0)}{k} = \frac{F_0}{k}; \tag{5}$$

$$\sigma_Q = \frac{1}{F_0} \int_0^{k_0} \frac{F_0}{k} \sigma(k)\, dk; \qquad (6)$$

$$= \int_0^{k_0} \frac{\sigma(k)}{k} dk;$$

$$\frac{d\sigma_Q(k_0)}{kd_0} = \frac{\sigma(k_0)}{k_0}; \qquad (7)$$

or

$$\sigma(k_0) = \frac{d\sigma_Q(k_0)}{d(\ln k_0)}, \quad \text{QED} \qquad (8)$$

BIBLIOGRAPHY

1. D.H.T. Grant, Nature 144, 707 (1939).
2. I.C. Jacobsen and N.O. Lassen, Phys. Rev. 58, 867 (1940).
3. G. Dessauer and E.M. Hafner, Phys. Rev. 59, 840 (1941).
4. E. Fermi and E. Segrè, Phys. Rev. 59, 680 (1941).
5. I. Perlman, R.H. Goeckermann, D.H. Templeton, and J.J. Howland, Phys. Rev. 72, 352 (1947).
6. R.H. Goeckermann and I. Perlman, Phys. Rev. 73, 1127 (1948).
7. P.R. O'Connor and G.T. Seaborg, Phys. Rev. 74, 1189 (1948).
8. A.S. Newton, Phys. Rev. 75, 17 (1949).
9. R.H. Goeckermann and I. Perlman, Phys. Rev. 76, 628 (1949).
10. J.A. Jungerman, Phys. Rev. 79, 632 (1950).
11. R.E. Batzel and G.T. Seaborg, Phys. Rev. 82, 607 (1951).
12. S.G. Al-Salam, Phys. Rev. 84, 254 (1951).
13. D.H. Greenberg and J.M. Miller, Phys. Rev. 84, 845 (1951).
14. N. Sugarman, Phys. Rev. 86, 604 (1952).
15. J.L. Fowler, W.H. Jones, and J.H. Paehler, Phys. Rev. 88, 71 (1952).
16. H.A. Tewes and R.A. James, Phys. Rev. 88, 860 (1952).
17. W. Galbraith and W.J. Whitehouse, Phil. Mag. 44, 77 (1953).
18. W.F. Biller, Jr., "The Characteristics of Bismuth Fission Induced by 340-Mev Protons"(Thesis), Radiation Laboratory University of California, Report No. UCRL-2067 (1953).
19. W. John and W.F. Fry, Phys. Rev. 91, 1234 (1953).
20. R.W. Spence and G.P. Ford, Ann. Rev. of Nuclear Science 2, 399 (1953).
21. E.M. Douthett and D.H. Templeton, Phys. Rev. 94, 128 (1954).
22. B.L. Cohen, W.H. Jones, G.H. McCormick, and B.L. Ferrell, Phys. Rev. 94, 625 (1954).
23. M. Lindner and R.N. Osborne, Phys. Rev. 94, 1323 (1954).
24. G.N. Harding, AERE-N/R-1438 (1954).
25. G.H. McCormick and B.L. Cohen, Phys. Rev. 96, 722 (1954).
26. W. Nervick and G.T. Seaborg, Phys. Rev. 97, 1092 (1955).

BIBLIOGRAPH (Continued)

27. H.A. Tewes, Phys. Rev. 98, 25 (1955).
28. R.L. Folger, P.C. Stevenson, and G.T. Seaborg, Phys. Rev. 98, 107 (1955).
29. B.L. Cohen, B.L. Ferrell-Bryan, D.J. Coombe, and M.K. Hullings, Phys. Rev 98, 685 (1955).
30. P. Kruger and N. Sugarman, Phys. Rev. 99, 1459 (1955).
31. L.G. Jodra and N. Sugarman, Phys. Rev. 99, 1470 (1955).
32. W.H. Jones, A. Timnick, J.H. Paehler and T.H. Handley, Phys. Rev. 99, 184 (1955).
33. N.A. Perfilov, N.S. Ivanova, O.V. Lozhkin, V.I. Ostroumov, V.P. Shamov, 1955 Moscow Conference of the Academy of Sciences USSR on Peaceful Applications of Atomic Energy. Meetings of the Division of Chemical Sciences. p. 79.
34. A.P. Vinogradov, I.P. Alimarin, V.I. Baranov, A.K. Lavrukhina, T.V. Baranova, F.I. Pavlotskaya, A.A. Bragina, I.V. Yakovlev, ibid., p. 97.
35. B.V. Kurchatov, V.N. Mekhedov, M.Y. Kuznetzova, L.N. Kurchatova, ibid., p. 120.
36. H.G. Hicks, P.C Steveson, R.S Gilbert, and W.H. Hutchin, Phys. Rev. 100, 1284 (1955).
37. H.G. Hicks and R.S. Gilbert, Phys. Rev. 100, 1286 (1955).
38. H.M. Steiner and J.A. Jungerman, Phys. Rev. 101, (1956).
39. G.G. Baldwin and G.S. Klaiber, Phys. Rev. 71, 3 (1947).
40. N.O. Lassen, Phys. Rev. 75, 1762 (1949).
41. T. Jorgensen, "A Method of Making Thin Uranium Oxide Films on Platinum Foils", MDDC, 467 (1946).
42. W.C Bright, "Spiral Fission Chambers", MDDC, 91 (1946).
43. B.B. Rossi and H.H. Staub, "Ionization Chambers and Counters", New York, McGraw-Hill, 1949, p. 210.
44. O. Chamberlain, E. Segrè, and C. Wiegand, Phys. Rev. 83, 923 (1951).
45. R. Serber, Phys. Rev. 72, 1114 (1947).
46. G.P. Millburn, W. Birnbaum, W.E. Crandall, and L. Schecter, Phys. Rev. 95, 1268 (1955).
47. M. Lindner, private communication.

BIBLIOGRAPHY (Continued)

48. H. McManus and W. T. Sharp, private communication.
49. R A. Schmitt and N. Sugarman, Phys Rev. 89, 1155 (1953).
50. G. Bernardini, R. Reitz, and E. Segrè, Phys. Rev. 90, 573 (1953).
51. J. Gindler, "The Photofission of Heavy Elements", (Thesis) University of Illinois, (1954).
52. R.A. Schmitt and N. Sugarman, Phys. Rev. 95, 1250 (1954).
53. L. Katz, T.M. Kavanagh, A.G.W. Cameron, E.C Bailey, and J.W.T. Spinks, Phys. Rev. 99, 98 (1955).
54. R. Wilson, private communication.
55. V.Z. Peterson, private communication.
56. C.A. McDonald, "Pair Production in the Field of Orbital Electrons by a Total Absorption Method at 300 Mev, (Ph.D. Thesis), (1954); University of California, Radiation Laboratory Report No. UCRL-2595.
57. V.Z. Peterson, private communication.
58. L.I. Schiff, Phys. Rev. 70, 87 (1946); Phys. Rev. 83, 252 (1951).
59. L. Katz and A.G.W. Cameron, Can. J. Phys. 29, 518 (1951).
60. D.C. Oakley and R.L. Walker, Phys. Rev. 97, 1283 (1955).
61. R L. Walker, D.C. Oakley and A.V. Tollestrup, Phys Rev. 97, 1279 (1955).
62. R.L. Walker, J.G. Teasdale, V.Z. Peterson, and J.I. Vette, Phys. Rev. 99, 210 (1955).
63. A.V. Tollestrup, J.C. Keck, and R.M. Worlock, Phys. Rev. 99, 220 (1955).
64. D.H. Stork, Phys. Rev. 93, 868 (1954).
65. C. Chedester, P. Isaacs, A. Sachs, and J. Steinberger, Phys. Rev. 82, 958 (1951).
66. R.M. Littauer and D. Walker, Phys. Rev. 86, 838 (1952).
67. W. Panofsky, J. Steinberger and J. Stellar, Phys. Rev. 86, 180 (1952).
68. A. Shapiro, Phys. Rev. 84, 1063 (1951).
69. K. Button, Phys. Rev. 88, 956 (1952).

BIBLIOGRAPHY (Continued)

70. G. Bernardini, E. Booth, and L. Lederman, Phys. Rev. 83, 1075 and 1277 (1951).

71. R. Martin, Phys. Rev. 87, 1052 (1952).

72. Y. Goldschmidt-Clermont, L. S. Osborne, and M. Scott, Phys. Rev. 97, 188 (1955).

73. V. Z. Peterson, private communication.

74. H. W. Koch, J. McElhinney, and E. L. Gasteiger, Phys. Rev. 77, 329 (1950).

75. J. M Blatt and V. F. Weisskopf, Theoretical Nuclear Physics, New York, Wiley, Ch. XII, p. 583.

76. Metropolis and Reitwiesner, "Table of Atomic Masses" US AEC Report NP-1980 (1950).